



**HAL**  
open science

# A comprehensive kinetic study on the speciation from propylene and propyne pyrolysis in a single-pulse shock tube

Wenyu Sun, Alaa Hamadi, Said Abid, Nabiha Chaumeix, Andrea Comandini

► **To cite this version:**

Wenyu Sun, Alaa Hamadi, Said Abid, Nabiha Chaumeix, Andrea Comandini. A comprehensive kinetic study on the speciation from propylene and propyne pyrolysis in a single-pulse shock tube. *Combustion and Flame*, 2021, 231, pp.111485. 10.1016/j.combustflame.2021.111485 . hal-03431148

**HAL Id: hal-03431148**

**<https://hal.science/hal-03431148v1>**

Submitted on 16 Nov 2021

**HAL** is a multi-disciplinary open access archive for the deposit and dissemination of scientific research documents, whether they are published or not. The documents may come from teaching and research institutions in France or abroad, or from public or private research centers.

L'archive ouverte pluridisciplinaire **HAL**, est destinée au dépôt et à la diffusion de documents scientifiques de niveau recherche, publiés ou non, émanant des établissements d'enseignement et de recherche français ou étrangers, des laboratoires publics ou privés.



# A comprehensive kinetic study on the speciation from propylene and propyne pyrolysis in a single-pulse shock tube

Wenyu Sun<sup>a,\*</sup>, Alaa Hamadi<sup>a</sup>, Said Abid<sup>a,b</sup>, Nabih Chaumeix<sup>a</sup>, Andrea Comandini<sup>a,\*</sup>

<sup>a</sup> CNRS-INSIS, I.C.A.R.E., 1C, Avenue de la recherche scientifique, 45071 Orléans cedex 2, France

<sup>b</sup> Université d'Orléans, 6 Avenue du Parc Floral, 45100 Orléans, France



## ARTICLE INFO

### Article history:

Received 13 January 2021

Revised 24 April 2021

Accepted 24 April 2021

### Keywords:

Propylene

Propyne

Pyrolysis

Aromatic hydrocarbons

Single-pulse shock tube

## ABSTRACT

This work is centered on the speciation from propylene and propyne pyrolysis by means of shock tube experiments and detailed kinetic modeling. A wealth of intermediates and products, covering small acyclic hydrocarbons up to four-ring aromatics, are probed from the C<sub>3</sub> fuels pyrolysis at a nominal pressure of 20 bar over 1050–1650 K. With updates in reactions involving C<sub>3</sub> species, our on-going polycyclic aromatic hydrocarbon (PAH) formation kinetic model can well predict the measurements obtained in the current work as well as relevant literature data. Propyne exhibits a unique two-stage decomposition profile, as the characteristic isomerization to allene dominates in its consumption at moderate temperatures below 1300 K. Overall, propylene pyrolysis results in more diverse small hydrocarbons, but much lower contents of aromatics, in comparison to propyne pyrolysis. In both studied cases, the formation of benzene is dependent upon the propargyl recombination, and since propyne decomposition induces a more rapid and more plentiful propargyl production, benzene mole fractions are much higher in propyne pyrolysis. In both cases, naphthalene is observed as the most abundant PAH species, followed by acenaphthalene. Modeling analyses indicate that similar reaction pathways are responsible for the PAH formation in propylene and propyne pyrolysis. Indene is formed from the interactions between benzene/phenyl and C<sub>3</sub> species, through its non-PAH isomers as intermediates. The subsequent reactions of indenyl radical with methyl and propargyl are essential pathways leading to naphthalene and acenaphthalene, respectively. Naphthyl radical further participates in the formation of different larger PAHs. The methylene-substituted cyclopenta-ring species are deemed as important precursors of their aromatic isomers, as is noted from the fulvene-to-benzene, benzofulvene-to-naphthalene and 9-methylene-fluorene-to-phenanthrene conversions.

© 2021 The Author(s). Published by Elsevier Inc. on behalf of The Combustion Institute.

This is an open access article under the CC BY-NC-ND license

(<http://creativecommons.org/licenses/by-nc-nd/4.0/>)

## 1. Introduction

Propylene and propyne are usually present in abundance among the combustion products of practical or surrogate fuels. The further dissociation of the C<sub>3</sub> molecules brings about resonantly stabilized radicals such as allyl and propargyl. These C<sub>3</sub> species are involved in important pathways leading to the production of the “first aromatic ring” [1–6], which is deemed as an essential step in the formation of polycyclic aromatic hydrocarbons (PAHs) and soot. Moreover, the formed aromatics can subsequently react with the C<sub>3</sub> species to gain larger aromaticity [7–11]. Towards the construction of a kinetic model that can predict the PAH formation

from combustion processes, it is elemental to accurately characterize the consumption of propylene and propyne and the subsequent molecular weight growth processes. Pyrolytic conditions offer the possibility of highlighting the break-down of fuel molecules and the build-up of PAH species, and corresponding quantitative speciation measurements provide crucial evidence in proposing the responsible reaction schemes.

Given the significance, pyrolysis kinetics of the propylene and propyne has been long pursued [12–28], and among numerous previous studies, some reported detailed speciation measurements, as summarized in Table 1. Various experimental configurations and techniques were used for the acquisition of the data sets covering different pressure, temperature and initial fuel concentration conditions. Back to 1970s, Burcat et al. [13] studied the cracking of propylene in a single-pulse shock tube and derived the first-step decomposition rate, by monitoring the production of stable small

\* Corresponding authors.

E-mail addresses: [wenyu.sun@cnrs-orleans.fr](mailto:wenyu.sun@cnrs-orleans.fr) (W. Sun), [andrea.comandini@cnrs-orleans.fr](mailto:andrea.comandini@cnrs-orleans.fr) (A. Comandini).

**Table 1**  
Literature studies reporting detailed speciation measurements from propylene and propyne pyrolysis.

Literature	Facility	Conditions
Propylene (C <sub>3</sub> H <sub>6</sub> )		
Burcat [13], 1975	shock tube	0.4% and 1.6% C <sub>3</sub> H <sub>6</sub> in Ar, $T = 1160 - 1700$ K, $p = 1.3 - 2.9$ atm, 5.5–8.8 atm, $\tau^* = 690 - 910$ $\mu$ s
Hidaka et al. [19], 1992	shock tube	2.5% and 5.0% C <sub>3</sub> H <sub>6</sub> in Ar, $T = 1200 - 1800$ K, $p = \sim 2$ atm; $\tau = 800 - 2500$ $\mu$ s
Davis et al. [20] 1999	flow reactor	0.288% C <sub>3</sub> H <sub>6</sub> in N <sub>2</sub> , $T = 1210$ K, $p = 1$ atm; $\tau = 0 - 200$ ms
Norinaga, et al. [22], 2008	flow reactor	C <sub>3</sub> H <sub>6</sub> without dilution, $T = 1073 - 1373$ K, $p = 8$ kPa; $\tau = 0.5$ s
Wang et al. [25], 2015	flow reactor	50% C <sub>3</sub> H <sub>6</sub> diluted in N <sub>2</sub> , $T = 848 - 1148$ K, $p = -0.83$ atm; $\tau = 2.4, 1.2$ and $0.5$ s
Nagaraja et al. [26], 2020	shock tube	2% C <sub>3</sub> H <sub>6</sub> diluted in Ar, $T = 1200 - 1800$ K, $p = 2$ atm; $\tau = 2.8 - 4.4$ ms
Propyne (C <sub>3</sub> H <sub>4</sub> -P)		
Hidaka et al. [17] 1989	shock tube	4.0% C <sub>3</sub> H <sub>4</sub> -P in Ar, $T = 1200 - 1570$ K, $p = 1.7 - 2.6$ atm; $\tau = 1800 - 2400$ $\mu$ s
Davis et al. [21] 1999	flow reactor	0.297% C <sub>3</sub> H <sub>4</sub> -P in N <sub>2</sub> , $T = 1210$ K, $p = 1$ atm; $\tau = 0 - 200$ ms
Panigrahy et al. [27] 2021	shock tube	2% C <sub>3</sub> H <sub>4</sub> -P diluted in Ar, $T = 1000 - 1600$ K, $p = 2$ bar; $\tau = 2.8 - 4.1$ ms

\*  $\tau$  is the reaction time in shock tube experiments and residence time in flow reactor experiments.

hydrocarbon products with a gas chromatography. In early 1990s, Hidaka et al. carried out a series of works to address the decomposition of small hydrocarbons including propylene [19] and propyne [17]. Infrared emission spectroscopy and gas chromatography techniques were combined to analyze the chemical compositions of the gas-mixtures behind reflected shock waves, and rate expressions for important reactions were evaluated. Davis et al. [20,21] reported time-dependent speciation measurements in propylene and propyne pyrolysis at 1210 K and atmospheric pressure in a flow reactor. RRKM rate coefficients were determined for specific reactions and used in detailed reaction mechanisms, which were later integrated in the widely-used USCMech II [29]. Norinaga et al. [22] and Wang et al. [25] both studied propylene pyrolysis in plug-flow reactors and provided species concentrations measurements as a function of the temperature. However, the two works [22,25], in which separate apparatus were employed, focused on different aspects: the former [22] also conducted pyrolysis experiments of ethylene and acetylene, and the obtained data were used to verify a proposed kinetic model; the later [25] aimed at developing a fundamentally-based kinetic model by incorporating theoretically determined rate coefficients for various types of reactions. Very recently, to provide validations for the newly-proposed core mechanism NUIMech1.0, concentration profiles of C<sub>0</sub>–C<sub>4</sub> species and benzene were measured from propylene [26] and propyne [27] pyrolysis using a new single-pulse shock tube facility.

Nevertheless, on the basis of the above review, new studies following specific orientations are still necessary on the “old topic” of propylene and propyne pyrolysis: first, most of the previous studies focused on the C<sub>3</sub> fuel decomposition reactivity and the formation of small hydrocarbons. Speciation measurements for heavy species like PAHs are relatively scarce, though highly required for the development of clean combustion techniques; Second, in the few studies [22,25] which reported PAH concentrations, the experiments were limited to sub-atmospheric pressure conditions and small temperature ranges below 1400 K. It is essential to extend the PAH measurements to larger temperature regimes and high pressure conditions that are more relevant to the practical operation conditions in combustion devices. Hence, in this work, high-pressure (~20 bar) shock tube pyrolysis experiments of propylene and propyne are carried out over a temperature range of 1050–1650 K. By employing the gas chromatography/gas chromatography-mass spectrometry (GC/GC-MS) techniques, a variety of species are probed from the post-shock mixtures, ranging from small C<sub>1</sub>–C<sub>3</sub> hydrocarbons produced through C<sub>3</sub> fuels dissociation to four-ring PAH compounds. A kinetic model, which has been developed in our serial works [30–33] on PAH formation chemistry, is used to interpret the measurements, after updates in specific reactions involving C<sub>3</sub> species. The detailed speciation behaviors in propylene and propyne pyrolysis are illustrated based on a combination of experimental observations and kinetic

modeling interpretations. Particular emphasis is put on revealing the aromatic species formation from the small intermediates pools, and the similarities and differences in the two studied systems are elucidated through comparisons.

## 2. Shock tube pyrolysis experiments

Pyrolysis experiments of propylene and propyne are carried out with the single-pulse shock tube facility at ICARE, Orléans. Detailed descriptions of the set-up and experimental procedures have been well documented in our previous publications [30–33]. The driven section of the shock tube is 6.0 m long with an inner diameter of 78 mm. It is separated from the driver section (length: 3.7 m; inner diameter: 120 mm) by a double diaphragm section. The driven section is heated up at 90 °C to avoid condensation or absorption of heavy species. To run the shock tube in a single-pulse fashion, a dump tank with a volume of 150 L is placed on the driven section side near the diaphragm. Four pressure sensors (CHIMIE METAL A25L05B) are mounted along the side wall of the driven section. The intervals between the neighboring sensors are 150 mm and the last sensor is 82 mm away from the endwall. The pressure signals are used to calculate the incident shock wave velocity, which is subsequently used to determine the post-shock conditions  $T_5$  and  $p_5$  by solving the conservation equations with the ideal gas law and variable heat capacity ratio. The physical dimension of the pressure sensors introduces uncertainties in the correlation between the time when the pressure rise is observed and the corresponding location on the sensitive area of the sensors. The sensitive area extends around  $\pm 1$  mm with respect to the center of the sensor, so the maximum error in the distance between two neighboring sensors is 2 mm. Besides, the accuracy and the signal-to-noise ratio of the pressure sensors may result in further uncertainties in the calculated shock wave velocities, but such uncertainties should be minor in view of the steep and large rises in the pressure signals. Finally, the presence of shock wave attenuation (below 2.5% for most experiments) can also affect the correct estimation of  $T_5$ . Given all the mentioned factors, an uncertainty of  $\pm 30$  K is estimated in the calculated  $T_5$ . A PCB Piezotronics pressure sensor, shielded by a layer of room-temperature vulcanizing (RTV) silicone, is mounted on the endwall. The pressure history in each shock operation is recorded, from which the corresponding reaction time can be defined as the time interval between the arrival of the shock wave and the time point when the pressure decreases to 80%  $p_5$  due to the quenching rarefaction waves. Two pressure profiles at different conditions, as well as the corresponding definition of reaction time, are presented in Fig. S1 as examples. The nominal reaction time with the current experimental configuration is 4.0 ms. An air-actuated valve is paced at the center of the endwall, and its operation is triggered by the endwall pressure signal, with a delay set at 4.0 ms, equivalent to the nom-

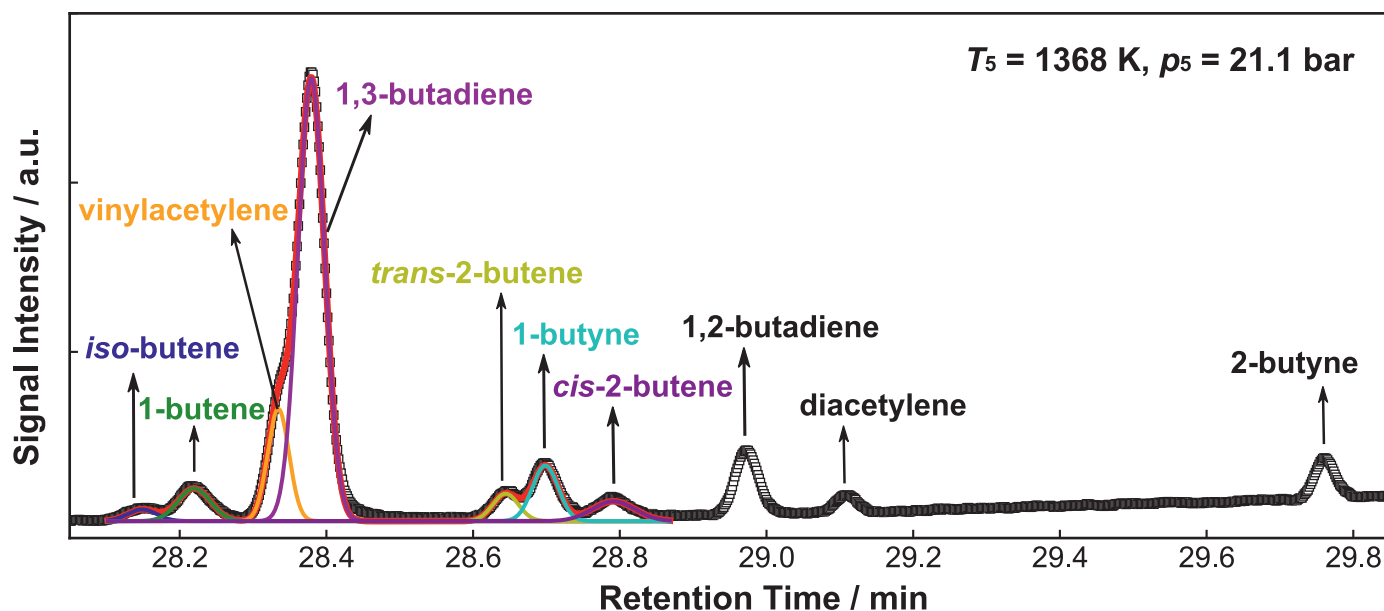


Fig. 1. The signals detected for  $C_4$  species in propylene pyrolysis at  $T_5 = 1368$  K,  $p_5 = 21.1$  bar. The overlapping peaks are separated through multiple gaussian fittings.

inal reaction time. The opening and closing of the sampling valve takes hundreds of milliseconds, resulting in a relatively large sample volume so that trace PAH species at the level of  $10^{-2}$  ppm can be detected. The sampled gas mixture is transferred to the analytical system through SilcoTek tubes, which are heated up at  $250$  °C to avoid condensation of the heavy products. Two GCs placed in series are used to analyze the chemical compositions of the post-shock gas samples. The first GC (Agilent 7890) is equipped with a flame ionization detector (FID) connected to a DB-17-ms column for separation and detection of the PAH species, while a thermal conductivity detector (TCD) with a Molsieve 5A column is used to monitor the absence of air. An external valve box, which can regulate the temperature up to  $320$  °C, is used for this GC to minimize the loss of heavy species during transportation and injection. An FID, coupled to an HP-PLOT Q column, is mounted on the second GC (Thermo Trace GC Ultra) to quantify the small species, mainly  $C_1$ – $C_6$  acyclic hydrocarbons and monocyclic aromatics in the current work. Various  $C_4$  species are observed in the current experiments, particularly in propylene pyrolysis. The signal recorded in propylene pyrolysis at  $T_5$  of  $1368$  K and  $p_5$  of  $21.1$  bar is shown in Fig. 1. A split injection mode (with a split ratio of 10) is used so that the signals exhibit good symmetrical Gaussian peak shapes. The overlapping peaks of the  $C_4$  species with close retention time are separated through multiple gaussian fittings. A DSQ mass spectrometer is also connected to the second GC to assist the identification of the PAH species. Before the experiments, different PAH standards are injected into the first GC to acquire their retention time, which is the main basis of the PAH identification. Meanwhile, the mass spectrometry provides essential information, such as the mass number of the detected species, and suggests possible isomeric candidates based on the ionization fragmentation patterns.

Regarding the quantification of the measured species, calibrations for the FID responses are conducted before the experiments. For the small hydrocarbons except diacetylene ( $C_4H_2$ ) and triacetylene ( $C_6H_2$ ), the calibrations are performed with standard gas mixtures with known compositions. The calibration for  $C_4H_2$  and  $C_6H_2$  is through high-temperature acetylene ( $C_2H_2$ ) pyrolysis experiments based on the carbon atom balance. To obtain accurate quantitative profiles of PAH species, the following procedures are followed to calibrate the FID response for PAH species up to three rings: i,) known amounts of PAH standards are dissolved in

dichloromethane to prepare the calibration solutions; ii,) a small dose of a calibration solution is injected with a syringe into a vacuumed glass vessel. The vessel is heated up at  $150$  °C so that the solution vaporizes immediately; iii,) the vessel is then filled with argon to around  $1.2$  bar, and the resulting PAHs-containing gas mixture stays for  $15$ – $20$  min to homogenize; iv,) the gas mixture is injected into the GC to obtain the normalized FID responses and this step is repeated for at least three times to ensure a good consistency; v,) the above procedures are conducted with several calibration solutions containing different PAH mole fractions that cover the range required in the experiments, and the calibration factors are derived for target PAH species. The calibration curves for a few typical two- to three- ring PAHs are provided in Fig. S2 in the *Supplementary Material*. The pressure-normalized peak areas are plotted against the mole fractions of individual calibrated PAH species, so the slope of the linear regression is the desired calibration factor. The calibration curves for the PAHs up to three rings, namely phenanthrene and anthracene, have good linearity. The above-mentioned gas-phase calibration approach, however, cannot be applied to four-ring or larger PAH species such as pyrene, because the complete vaporization cannot be guaranteed. Therefore, the corresponding calibration factors are obtained based on the extrapolation of the one- to three- ring aromatics, *i.e.* benzene, naphthalene and phenanthrene. The uncertainty in the measured species mole fractions mainly come from the errors in the calibration. The uncertainty is estimated to be within  $5\%$  for the directly calibrated small species, and increases to  $10\%$ – $15\%$  for the indirectly calibrated  $C_4H_2$ ,  $C_6H_2$  and the PAH species calibrated in gas phase; while for the heavier PAHs which cannot be calibrated in gas phase, the uncertainty may be as large as  $50\%$  or even more.

The  $C_3$  fuel gases used in the experiments, propylene ( $99.5\%$ ) and propyne ( $97\%$ ), are provided by Air Liquide and Sigma-Aldrich, respectively. The main impurities are analyzed to be propane in propylene and 2-butene and iso-butane in propyne. Other gases including argon ( $>99.9999\%$ ) and helium ( $99.995\%$ ) and the mixtures for small species calibration are supplied by Air Liquide; The PAH samples are purchased from Sigma-Aldrich. The experimental gas mixtures are prepared in a  $136$  L electropolished stainless steel cylinder which is evacuated to below  $10^{-5}$  mbar with a turbomolecular pump in advance. Propylene or propyne is introduced to the cylinder to a partial pressure of around  $3.75$  Torr, monitored

by a MKS Baratron pressure transducer with the measuring range of 0–10 Torr; the cylinder is then filled with argon to a total pressure of about 7500 Torr, measured by a 0–10,000 Torr MKS Baratron pressure transducer. Before the experiments, the prepared gas mixtures stay overnight to homogenize, and the actual compositions are analyzed with the GC. The two experimental mixtures used in the current work separately contain 518 ppm propylene and 509 ppm propyne. In each experiment, the pressure in the driven section of the shock tube is pumped to below  $10^{-5}$  mbar before being filled with the experimental mixture. The inner surface of the driven section is cleaned every day to remove carbon deposit produced from the experiments. All experimental results, consisting of the post-shock conditions  $T_5$ ,  $p_5$ , the measured pressure profiles, the defined reaction time, as well as mole fraction measurements for individual species, are provided in the *Supplementary Material*.

### 3. Kinetic modeling

The current work is a continuation of our previous serial works [30–33] towards building a kinetic model that accurately predicts the PAH formation in the pyrolysis of practical/surrogate fuels. It started with the PAH formation mechanism from the basic aromatics such as benzene and toluene [30], and the speciation in larger  $C_8$ – $C_{10}$  alkylbenzenes pyrolysis was further inspected [32]. The binary aromatic/ $C_2$  mixtures were also studied [31,33], so that interactions between aromatic radicals and small  $C_2$  hydrocarbons could be highlighted. Similar to the  $C_2$  hydrocarbons, the  $C_3$  hydrocarbons are also basic intermediates from larger fuels' consumption and extensively involved in the build-up of PAH species. Since the latest CRECK PAH model by Pejpichestakul et al. [34] was selected as the starting point of our model development [30], the  $C_3$  sub-mechanism is already included in the core mechanism of the on-going kinetic model. Rate coefficients for propylene ( $C_3H_6$ ) and propyne ( $C_3H_4$ -P) unimolecular decomposition reactions and the  $C_3H_6/C_3H_4$ -P+H reactions mostly originate from the theoretical analyses on the  $C_3H_{4-7}$  potential energy surfaces (PESs) in the publications by Klippenstein and coworkers [35–38]. In addition, the reaction between singlet methylene and acetylene ( $^1CH_2 + C_2H_2 = C_3H_4$ -P) [39] is included in the kinetic model, as the reverse reaction potentially contributes to propyne dissociation. The corresponding fuel radicals of  $C_3H_6$  and  $C_3H_4$ -P, in particular, the resonantly-stabilized allyl ( $C_3H_5$ -A) and propargyl ( $C_3H_3$ ), are important benzene precursors in the combustion of acyclic fuels, and relevant kinetic processes have been extensively addressed in literature. Rate coefficients for the  $C_3H_3$  recombination reactions forming fulvene and benzene are from the theoretical work by Miller and Klippenstein [1]. The reactions of  $C_3H_3 + C_3H_4$ -P/ $C_3H_4$ -A =  $C_6H_6$ +H as well as the corresponding rate coefficients are from the CRECK PAH model [34] without modification. No theoretically determined rate coefficients for such reactions are available in literature to the best of our knowledge, and the one used in [34],  $k = 1.40 \times 10^{12} \exp(-10 \text{ kcal}/RT)$ , originates from an early study on propyne and allene pyrolysis by Hidaka et al. [17]. Given the role of these reactions as potential contributors to benzene formation, future theoretical works are necessary to enhance the accuracy of the kinetic parameters. The reaction  $C_3H_3 + C_3H_5$ -A = fulvene+2H, together with the rate coefficient reported in the work by Hansen et al. [2] is adopted to represent the formation of a hydrogen atom and a  $C_6H_7$  radical that subsequently decomposes to fulvene and another hydrogen atom [2]. The rate coefficient reported by Jasper and Hansen [40] is used for the hydrogen assisted isomerization of fulvene to benzene. Different from the case of  $C_3H_3$  self-recombination leading to cyclic species, the  $C_3H_5$ -A self-recombination is found to mainly produce the straight-chained 1,5-hexadiene ( $CH_2=CHCH_2CH_2CH=CH_2$ , DIAL-

LYL). Rate coefficients for this channel, as well as for a competing disproportionation reaction leading to  $C_3H_6 + C_3H_4$ -A, originate from the shock tube studies by Lynch et al. [41] and Fridlyand et al. [42], respectively. The  $CH_2=CHCH_2\dot{C}HCH=CH_2$  radical, which may be formed through the hydrogen abstraction of 1,5-hexadiene, appears on the  $C_6H_9$  reaction PES. This surface also includes the addition reactions of vinyl ( $C_2H_3$ )+1,3-butadiene ( $C_4H_6$ ) and  $C_3H_5$ -A+ $C_3H_4$ -P/ $C_3H_4$ -A and the formation/consumption of five-membered and six-membered cyclic species, such as cyclopentadiene ( $CYC_5H_6$ )+ $CH_3$ , methyl-cyclopentadiene ( $C_5H_5CH_3$ )+H and cyclohexadiene ( $CYC_6H_8$ )+H. Relevant reactions as well as the corresponding rate coefficients reported in [43] are incorporated in the current kinetic model. Reactions between  $C_3H_6$  and  $C_3H_5$ -A involved on the  $C_6H_{11}$  PES were studied by Wang et al. [25], and the resulting pathways and corresponding rate coefficients [25] are used in the current model. Since numerous  $C_4$  species are observed in the experiments, updates are also made in the  $C_4$  sub-mechanisms. For the decomposition and isomerization reactions of  $C_4H_6$  isomers (2-butyne, 1,2-butadiene and 1,3-butadiene), the rate coefficients acquired through an RRKM/master equation analysis by Huang et al. [44] are adopted. The decomposition reactions of another  $C_4H_6$  isomer, 1-butyne, are however not addressed in the theoretical work by Huang et al. [44]. So the rate coefficients of 1-butyne decomposition reactions reported in the shock tube study by Lockhart et al. [45] are used. Exceptions are made for specific reactions including the decompositions of 1,2-butadiene and 1-butyne to propargyl and methyl ( $C_4H_6$ -1,2/ $C_4H_6$ -1  $\rightarrow$   $C_3H_3 + CH_3$ ). The  $C_3H_3 + CH_3$  recombination reactions are used to represent the reversible processes, by employing the latest theoretical rate coefficients reported by Pham et al. [46]. Vinylacetylene ( $C_4H_4$ ) decompositions and relevant kinetic parameters originate from recent theoretical work by Zador et al. [47]. The reactions between  $C_3$  fuels and the  $C_2$  intermediates result in the formation of  $C_5$  species. Reactions on the  $C_5H_9$  PES, including  $C_3H_6 + C_2H_3$ ,  $C_3H_5$ -A+ $C_2H_4$ ,  $C_3H_4$ -P/ $C_3H_4$ -A+ $C_2H_3$ , reported by Wang et al. [25] are integrated in the current model. Cyclopentadienyl ( $C_5H_5$ ) is an important  $C_5$  radical, given its resonantly stabilized nature. The reactions between  $C_5H_5$  and  $CH_3$  result in the formation of  $C_6$  species, which may further lead to benzene and fulvene through dehydrogenation processes. Involved reactions and the corresponding reactions reported in [48,49] are used in the current model. Towards the formation of  $C_7$  species, in particular benzyl ( $C_7H_7$ ), the  $C_5H_5 + C_2H_2$  [50] and  $C_4H_4 + C_3H_3$  reactions [51], are considered in this work.

Following the formation of the first aromatic ring, the reactions between the  $C_3$  species and the aromatics such as benzene and phenyl further contribute to the formation of larger PAH species. The interactions between benzene (or phenyl) and  $C_3$  radicals (or molecules) are considered as an important source of indene [8,9,52–55]. By carrying out a systematic theoretical study on the reaction potential surfaces (PESs) of  $C_9H_{8-11}$ , Mebel and coworkers recently derived pressure-dependent rate coefficients for the molecule+radical reaction channels starting from phenyl+propyne ( $C_6H_5 + C_3H_4$ -P), phenyl+allene ( $C_6H_5 + C_3H_4$ -A), benzene+propargyl ( $C_6H_6 + C_3H_3$ ), phenyl+propylene ( $C_6H_5 + C_3H_6$ ) and benzene+allyl ( $C_6H_6 + C_3H_5$ -A) [8], and the radical+radical reactions of phenyl+propargyl ( $C_6H_5 + C_3H_3$ ) [11] and phenyl+allyl ( $C_6H_5 + C_3H_5$ -A) [10]. The reported reaction pathways and corresponding kinetic parameters [8,10,11] are included in the current model. The  $C_6H_5 + C_4H_4$  reactions forming naphthalene ( $C_{10}H_8$ ), as well as the competing channel forming the non-PAH  $C_6H_5C_4H_3$  species are also considered in the current model, and the rate coefficients reported by Mebel et al. [9] are used. In a similar manner, the reaction of naphthyl ( $C_{10}H_7$ ) and  $C_4H_4$  forming phenanthrene is also considered in the current model through an analogy to the reaction of  $C_6H_5 + C_4H_4 = C_{10}H_8 + H$ .



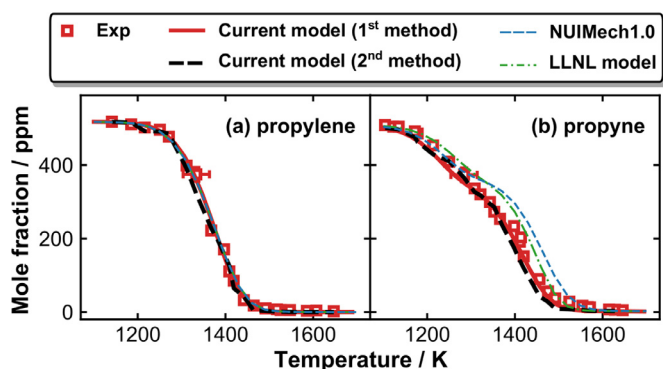


Fig. 2. Measured (symbols) and simulated (lines) fuel mole fraction profiles as a function of  $T_5$  in (a) propylene pyrolysis and (b) propyne pyrolysis. Thick solid red lines: simulations using the current kinetic model with the constant  $p_5$  of 20 bar and the nominal reaction time of 4 ms; thick dashed black lines: simulations using the current model with measured pressure profiles up to 10 ms; thin dashed blue lines: simulations using the NUIMech1.0 [26] for propylene and [27] for propyne) with the constant  $p_5$  of 20 bar and the nominal reaction time of 4 ms; thin dot dashed green lines: simulations using the LLNL PAH model [64] with constant  $p_5$  of 20 bar and the nominal reaction time of 4 ms.

The thermochemical data for most species in the current model are from the latest version of CRECK model [34], which originate from the databases of ATcT [56] or Burcat [57]. For the species that are missing from the CRECK model, thermochemical data are found in the Burcat's database [57] or computed with the program THERM [58]. The kinetic model, including the reaction mechanism and the species thermochemical data, is provided in the *Supplementary Material*. Simulations in the present work are performed with the homogeneous reactor model of the software COSILAB [59]. Two methods are used in simulating the speciation measurements with the current kinetic model: 1) simulations with a constant  $p_5$  of 20 bar and a nominal reaction time of 4 ms; 2) simulations with  $T_5$  at the zero time point and the measured pressure profiles up to 10 ms. The first method has been widely used in the simulations for speciation measurements sampled from single-pulse shock tubes [60,61], and the constant pressure assumption is well justified [62,63]. Nevertheless, the second method is necessary to take account of specific reactions involving resonantly stabilized radicals, which potentially proceed during the post-shock quenching. Recent kinetic models, including the NUIMech1.0 updated by Nagaraja et al. [26] and Panigrahy et al. [27] for the combustion of propylene and propyne, respectively, and the LLNL PAH model reported by Shao et al. [64], are also used to simulate the current experiments for comparison purpose. Although a lot of reactions are shared in the NUIMech and the LLNL models, recent updates were focused on different aspects, as mentioned above. Therefore, in the following section, the current model is compared with the NUIMech and the LLNL models mainly regarding the predictions for small hydrocarbons and aromatic species, respectively. The impurities are considered in the simulations, more specifically, 2 ppm propane in propylene pyrolysis, 4.5 ppm 2-butene and 3.5 ppm iso-butane in propyne pyrolysis.

To test the predictivity of the current kinetic model for propylene and propyne pyrolysis under different conditions, the model is validated against relevant speciation data reported in literature [13,17,19–21,25–27]. Different experimental configurations and thus corresponding simulation methods are involved. For the shock tube experiments [13,17,19,26,27], each data point is simulated with the homogeneous reactor by inputting the measured  $T_5$ ,  $p_5$  and reaction time. The "plug-flow" model is employed to simulate the speciation of propylene pyrolysis in a laminar flow tube pyrolysis [25]. The measured temperature profiles are used for individual conditions, and the species mole fractions at the exit

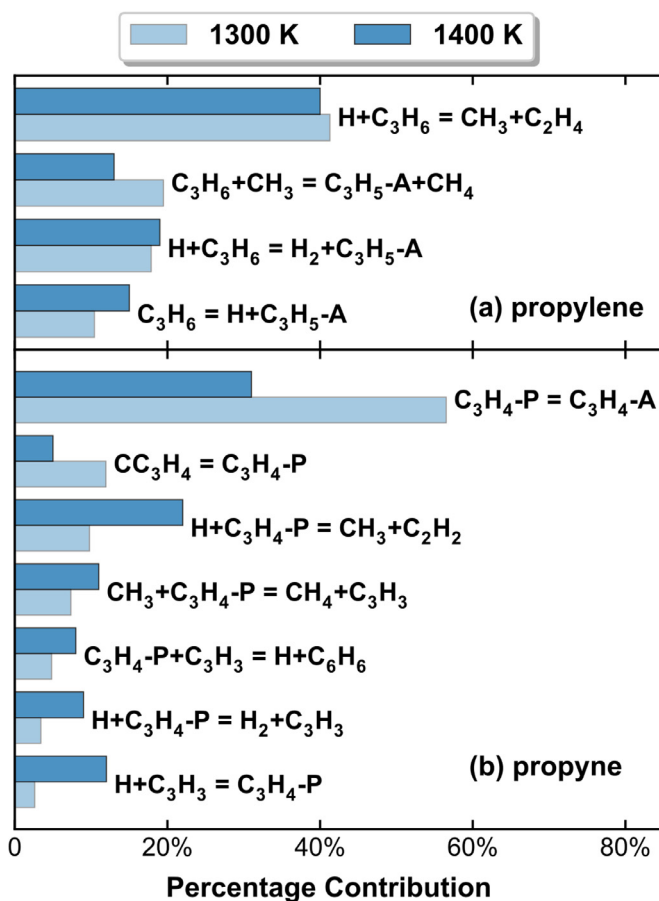
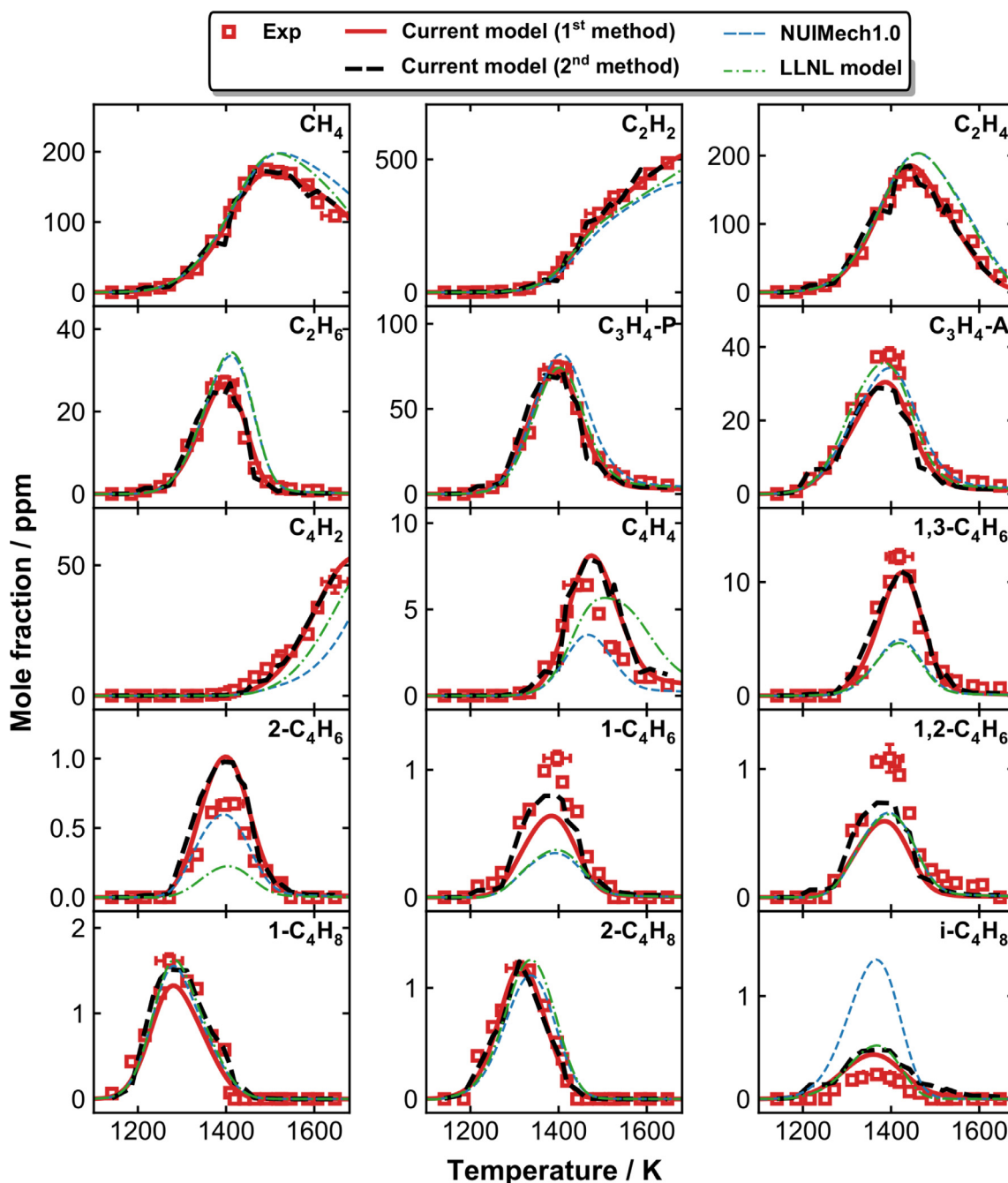


Fig. 3. Major fuel consumption pathways at  $T_5$  of 1300 K and 1400 K based on ROP-analyzed results.

of the reactor are extracted and plotted against the reactor temperatures (the approximately constant temperatures in the central region of the reactor). As for the experiments performed with the Princeton flow reactor [20,21], an isobaric and adiabatic zero-dimensional reactor is used by giving the initial temperature, pressure and chemical compositions to simulate the species mole fraction time histories. The comparisons between the literature data [13,17,19–21,25–27] and the simulations with the current model are presented in Figs. S3–S13 in the *Supplementary Material*.

#### 4. Results and discussion

In the current work, more than 40 species, including two- to four- ring PAH compounds, are identified and quantified in separate cases of propylene and propyne pyrolysis. Most detected species are shared in both cases, but with different abundance. The current kinetic model can well characterize the measured speciation data, as illustrated later in this section. Furthermore, the model can also satisfactorily predict literature data obtained under extensive conditions involving different experimental configurations, as can be observed in Figs. S3–S13. In this section, we first examine the fuel decomposition reactivity and the speciation of small intermediates, and then put emphasis on the production of aromatic species, from the simplest benzene to larger PAHs. The following discussion is organized through comparisons between the two cases of propylene and propyne pyrolysis. Influences of specific factors, such as the reactions during post-shock quenching, are also evaluated.



**Fig. 4.** Measured (symbols) and simulated (lines) small intermediates mole fraction profiles as a function of  $T_5$  in propylene pyrolysis. Thick solid red lines: simulations using the current kinetic model with the constant  $p_5$  of 20 bar and the nominal reaction time of 4 ms; thick dashed black lines: simulations using the current model with measured pressure profiles up to 10 ms; thin dashed blue lines: simulations using the NUIMech1.0 [26] with the constant  $p_5$  of 20 bar and the nominal reaction time of 4 ms; thin dot dashed green lines: simulations using the LLNL PAH model [64] with the constant  $p_5$  of 20 bar and the nominal reaction time of 4 ms. (For interpretation of the references to color in this figure legend, the reader is referred to the web version of this article.)

#### 4.1. Fuel decomposition and the formation of small hydrocarbons

Fig. 2 shows the fuel mole fraction profiles as a function of  $T_5$ , including measurements and simulations using different methods and with different kinetic models. Propylene decomposition follows a regular smooth curve, covering a temperature regime of 1200–1500 K. The decay of propyne, however exhibits unique behaviors, as it starts at around 1100 K then experiences two stages of consumption at distinct rates. This phenomenon is also clearly seen in propyne pyrolysis at a higher initial mole fraction (4%) and lower pressures around 2 atm [17]. The current model, as

well as the literature models [27,64], can well predict such unique fuel conversion processes (see Fig. 2(b)). The post-shock quenching does not obviously influence the fuel decomposition, as the simulations with the current model using two different methods give similar results.

Major fuel consumption pathways (reactions with a contribution over 5%) of propylene and propyne pyrolysis at 1300 K and 1400 K are summarized in Fig. 3, based on rate-of-production (ROP) analyses. At both analyzed temperatures, the chemically-activated reaction  $H+C_3H_6 = CH_3+C_2H_4$  accounts for about 40% of propylene consumption, while the contributions of other three

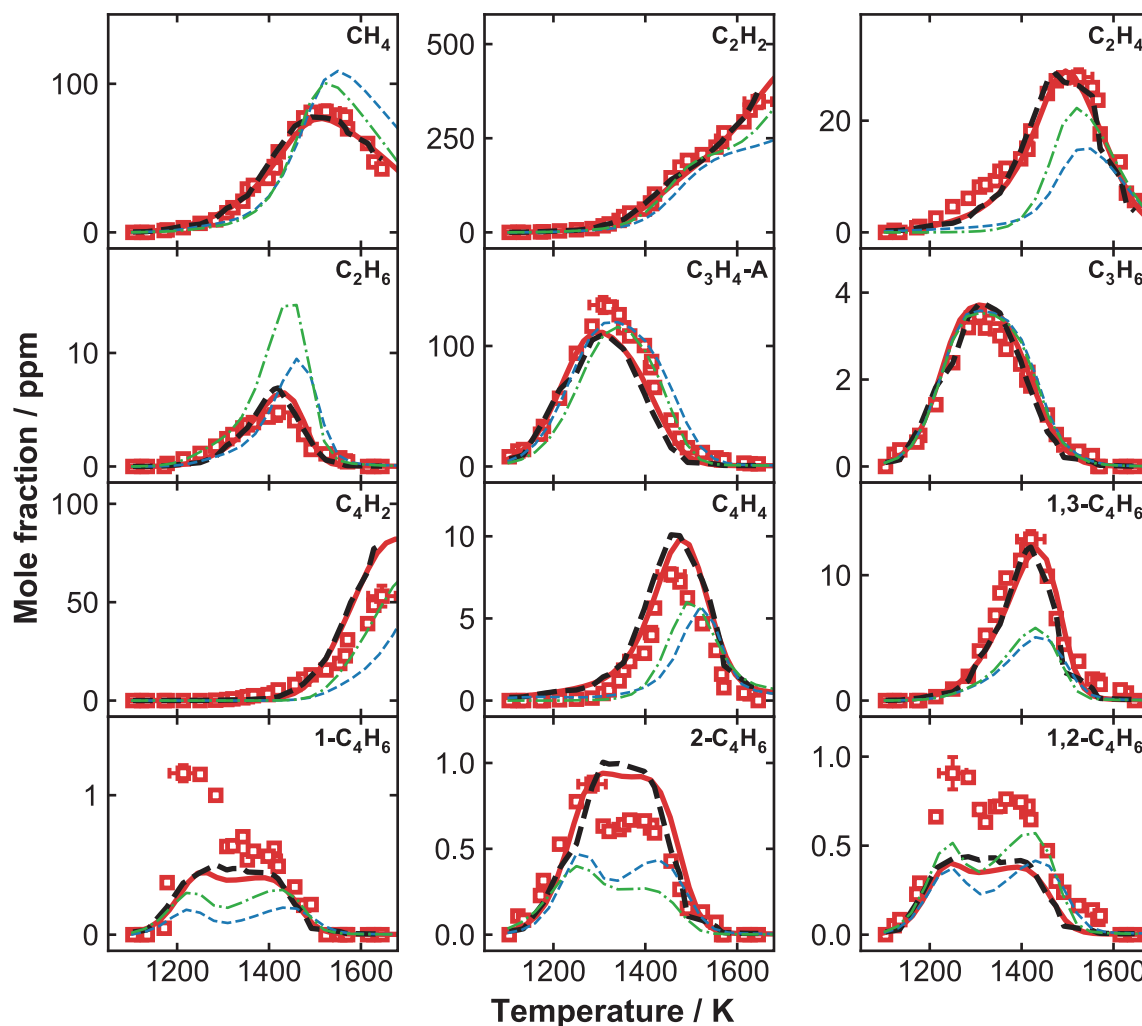


**Fig. 5.** Measured (symbols) and simulated (lines) small intermediates mole fraction profiles as a function of  $T_5$  in propyne pyrolysis. Thick solid red lines: simulations using the current kinetic model with the constant  $p_5$  of 20 bar and the nominal reaction time of 4 ms; thick dashed black lines: simulations using the current model with measured pressure profiles up to 10 ms; thin dashed blue lines: simulations using the NUIMech1.0 [27] with the constant  $p_5$  of 20 bar and the nominal reaction time of 4 ms; thin dot dashed green lines: simulations using the LLNL PAH model [64] with the constant  $p_5$  of 20 bar and the nominal reaction time of 4 ms. (For interpretation of the references to color in this figure legend, the reader is referred to the web version of this article.)

channels slightly vary in a range of 10%–20%. Because of the sufficient  $\text{CH}_3$  production, the hydrogen abstraction by  $\text{CH}_3$  is the second most important  $\text{C}_3\text{H}_6$  consumption channel at 1300 K. The relative importance of the C–H bond fission forming allyl ( $\text{C}_3\text{H}_5\text{-A}$ ) and the hydrogen abstraction reaction by H increases at 1400 K. The reaction scheme of propyne decomposition is more sensitive to the temperature. At low temperatures, the isomerization to allene ( $\text{C}_3\text{H}_4\text{-A}$ ) dominates the consumption of propyne, corresponding to the first stage of decomposition as mentioned above. At higher temperatures, *i.e.* the second stage of propyne consumption, hydrogen atoms are released from the chain-initiating C–H bond fission (the reverse of  $\text{H}+\text{C}_3\text{H}_3 = \text{C}_3\text{H}_4\text{-P}$ ), so that the reaction  $\text{H}+\text{C}_3\text{H}_4\text{-P} = \text{CH}_3+\text{C}_2\text{H}_2$  becomes a significant fuel consumption pathway, and its contribution exceeds that of the isomerization ( $\text{C}_3\text{H}_4\text{-P} = \text{C}_3\text{H}_4\text{-A}$ ) above 1430 K. Due to the unsaturated nature of propylene and propyne, a larger portion of the  $\text{C}_3$  fuel is consumed through the addition-elimination channel  $\text{H}+\text{C}_3\text{H}_x = \text{CH}_3+\text{C}_2\text{H}_{x-2}$  ( $x = 6, 4$ ), instead of the competing hydrogen abstraction reactions.

Small hydrocarbons are formed directly from the fuel consumption pathways discussed above, or through the subsequent reactions. Temperature-dependent mole fraction profiles of small hydrocarbon intermediates and products, mainly  $\text{C}_1\text{-C}_4$  acyclic

species, in propylene and propyne pyrolysis are displayed in Figs. 4 and 5, respectively. Propyne is observed as an important intermediate in propylene pyrolysis, therefore the small products of propyne decomposition are also present in the species pool of propylene pyrolysis. The speciation of  $\text{C}_3\text{H}_4\text{-A}$  starts at a lower temperature than  $\text{C}_3\text{H}_4\text{-P}$ , as  $\text{C}_3\text{H}_4\text{-P}$  is produced from the  $\text{C}_3\text{H}_6\text{-A}$  isomerization, subsequent to the dehydrogenation process of  $\text{C}_3\text{H}_6 \rightarrow \text{C}_3\text{H}_5\text{-A} \rightarrow \text{C}_3\text{H}_4\text{-A}$ . In propyne pyrolysis, the temperature regime where  $\text{C}_3\text{H}_4\text{-A}$  starts to form till reaching the peak mole fraction synchronizes with that of the first stage of  $\text{C}_3\text{H}_4\text{-P}$  consumption. These observations suggest that the mutual isomerization is a fast process and the most important consumption pathways of propyne and allene at relatively low temperatures. The onset of methane ( $\text{CH}_4$ ) formation appears at relatively low temperatures in both cases, result from the hydrogen abstraction reactions by  $\text{CH}_3$  from the fuel molecules, following the  $\text{H}+\text{C}_3\text{H}_6$  (or  $\text{C}_3\text{H}_4\text{-P}$ ) =  $\text{CH}_3+\text{C}_2\text{H}_4$  (or  $\text{C}_2\text{H}_2$ ) reactions. The butene isomers are only observed in propylene pyrolysis. The formation of 1-butene ( $1\text{-C}_4\text{H}_8$ ) occurs at a relatively low temperature where propylene just starts to decompose. The  $\text{C}_3\text{H}_5\text{-A}+\text{CH}_3$  recombination and the reaction  $1\text{-C}_4\text{H}_8+\text{H} = \text{C}_3\text{H}_6+\text{CH}_3$ , give rise to the production of  $1\text{-C}_4\text{H}_8$ , and the latter channel ( $\text{C}_3\text{H}_6+\text{CH}_3$ ) also leads to the forma-



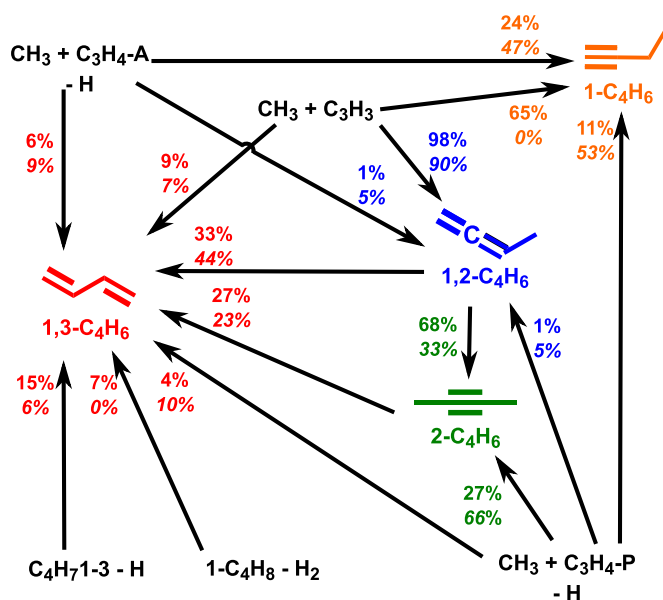


Fig. 6. Formation pathways of C<sub>4</sub>H<sub>6</sub> isomers at T<sub>5</sub> = 1400 K. The percentage numbers (normal font: in propylene pyrolysis; italic font: in propyne pyrolysis) represent the contributions of corresponding reactions to the formation of C<sub>4</sub>H<sub>6</sub> isomers.

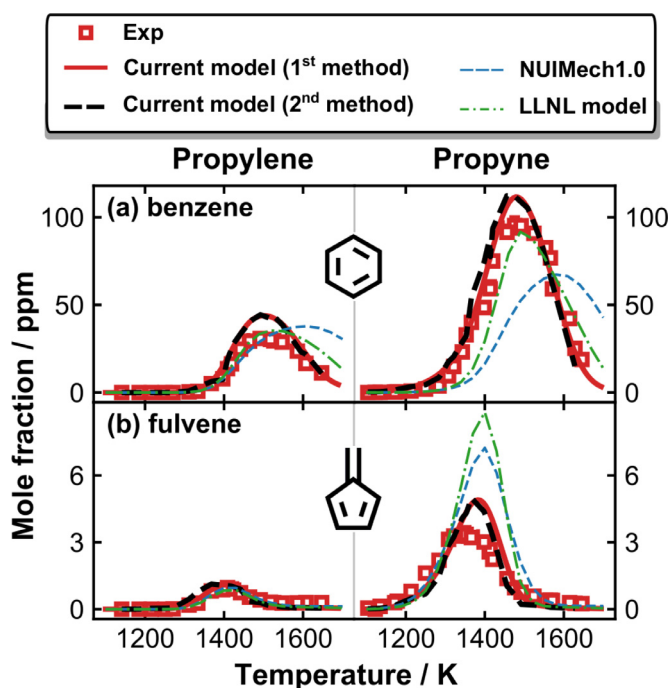


Fig. 7. Measured (symbols) and simulated (lines) benzene and fulvene mole fraction profiles as a function of T<sub>5</sub> in propyne pyrolysis. Thick solid red lines: simulations using the current kinetic model with the constant p<sub>5</sub> of 20 bar and the nominal reaction time of 4 ms; thick dashed black lines: simulations using the current model with measured pressure profiles up to 10 ms; thin dashed blue lines: simulations using the NUIMech1.0 [26] for propylene and [27] for propyne) with the constant p<sub>5</sub> of 20 bar and the nominal reaction time of 4 ms; thin dashed green lines: simulations using the LLNL PAH model [64] with constant p<sub>5</sub> of 20 bar and the nominal reaction time of 4 ms.

tion of 2-butene (2-C<sub>4</sub>H<sub>8</sub>) and iso-butene (i-C<sub>4</sub>H<sub>8</sub>). It is noteworthy that a part (about 15%) of 1-C<sub>4</sub>H<sub>8</sub> is formed during the quenching period, while the formation of the other two isomers (2-C<sub>4</sub>H<sub>8</sub> and i-C<sub>4</sub>H<sub>8</sub>) is completed during the reaction time of 4 ms. The reason lies in that the radical recombination process between C<sub>3</sub>H<sub>5</sub>-A and

CH<sub>3</sub>, which dominates the formation 1-C<sub>4</sub>H<sub>8</sub>, continues after the arrival of the rarefaction waves.

Four C<sub>4</sub>H<sub>6</sub> isomers, 1-butyne (1-C<sub>4</sub>H<sub>6</sub>), 2-butyne (2-C<sub>4</sub>H<sub>6</sub>), 1,2-butadiene (1,2-C<sub>4</sub>H<sub>6</sub>) and 1,3-butadiene (1,3-C<sub>4</sub>H<sub>6</sub>) are observed in propylene and propyne pyrolysis. 1,3-C<sub>4</sub>H<sub>6</sub> is the dominant one, with the peak mole fractions one order of magnitude higher than the other three isomers. Quantitative mole fraction profiles of well-resolved C<sub>4</sub>H<sub>6</sub> isomers are scarcely reported in previous studies concerning propylene and propyne pyrolysis. In both propylene and propyne pyrolysis, the simulated mole fractions of 1-C<sub>4</sub>H<sub>6</sub> and 1,2-C<sub>4</sub>H<sub>6</sub> are higher when using the pressure profiles, indicating that their formation continues during the post-shock quenching. The current model can well capture the mole fraction measurements for 1,3-C<sub>4</sub>H<sub>6</sub>, though discrepancies exist between the experimental and simulated speciation profiles of the three other isomers. Fig. 6 displays the formation pathways of the C<sub>4</sub>H<sub>6</sub> isomers based on ROP analyses at 1400 K, where 1,3-C<sub>4</sub>H<sub>6</sub> mole fraction reaches the peak. Reactions between CH<sub>3</sub> and C<sub>3</sub> molecules/radicals (C<sub>3</sub>H<sub>4</sub>-P, C<sub>3</sub>H<sub>4</sub>-A and C<sub>3</sub>H<sub>3</sub>) govern the formation of C<sub>4</sub>H<sub>6</sub> isomers. The formation of the dominant isomer 1,3-C<sub>4</sub>H<sub>6</sub> largely relies on the isomerization reactions of 1,2-C<sub>4</sub>H<sub>6</sub>, which mainly comes from the CH<sub>3</sub>+C<sub>3</sub>H<sub>3</sub> recombination. Kinetics of this barrierless radical + radical recombination processes was addressed in literature [46,65,66], and it was consistently concluded that 1-C<sub>4</sub>H<sub>6</sub> and 1,2-C<sub>4</sub>H<sub>6</sub> are the major products, especially under the currently concerned high-pressure and high-temperature conditions [46]. In propylene pyrolysis, the consumption of 1-C<sub>4</sub>H<sub>8</sub> also contributes to 1,3-C<sub>4</sub>H<sub>6</sub> formation, through H<sub>2</sub> elimination and the step-wise dehydrogenation via C<sub>4</sub>H<sub>7</sub>-1-3 radical (CH<sub>2</sub>=CHCHCH<sub>3</sub>) as an intermediate. Though 1-C<sub>4</sub>H<sub>8</sub> is absent from the products pool of propyne pyrolysis, 6% of 1,3-C<sub>4</sub>H<sub>6</sub> formation is contributed by the decomposition of C<sub>4</sub>H<sub>7</sub>-1-3, which alternatively comes from the impurity 2-C<sub>4</sub>H<sub>8</sub> decomposition.

The measured mole fraction profiles of the minor C<sub>4</sub>H<sub>6</sub> isomers (1-C<sub>4</sub>H<sub>6</sub>, 2-C<sub>4</sub>H<sub>6</sub> and 1,2-C<sub>4</sub>H<sub>6</sub>) exhibit double-peak shapes. The decreasing trends over the temperature range of 1200–1300 K can be captured by the literature models, while the current model cannot reproduce such phenomena. ROP analyses with the LLNL PAH model suggest that the decreases in 1-C<sub>4</sub>H<sub>6</sub>, 2-C<sub>4</sub>H<sub>6</sub> and 1,2-C<sub>4</sub>H<sub>6</sub> mole fractions are mainly due to the reduced formation through C<sub>3</sub>H<sub>3</sub>+CH<sub>3</sub> and the increased conversion to 1,3-C<sub>4</sub>H<sub>6</sub>. The current model can also predict the increased consumption through the isomerization to 1,3-C<sub>4</sub>H<sub>6</sub>, but the formation through C<sub>3</sub>H<sub>3</sub>+CH<sub>3</sub> increases as well. The above-mentioned reactions are involved in a C<sub>4</sub>H<sub>6</sub> PES, and the corresponding rate coefficients are taken from recent theoretical works [44,46] in the current model, as mentioned in the kinetic modeling section. The radical+radical recombination and the isomerization reactions can be largely influenced by the used thermochemical data. The thermochemical data for the four C<sub>4</sub>H<sub>6</sub> isomers come from a consistent source, the Burcat database [57], in the current model, while those in the literature kinetic models [26,27,64] were computed using THERM [58] or derived from literature [67]. If the thermochemical data for C<sub>4</sub>H<sub>6</sub> isomers from the LLNL or the NUIMech model are used in the current model, the predicted mole fractions of 1,3-C<sub>4</sub>H<sub>6</sub> will decrease by half. The selection for both kinetic and thermochemical data in the current model results in a good prediction for the mole fraction distribution of the dominant 1,3-C<sub>4</sub>H<sub>6</sub>, though the predictions for the minor isomers are less satisfactory. Improvements are needed in the sub-mechanisms of the C<sub>4</sub>H<sub>6</sub> isomers, by refining both the kinetic and thermochemical parameters in future works.

#### 4.2. Formation of the “first aromatic ring”

The formation of benzene is one of the major topics discussed in kinetic studies of acyclic fuels consumption under fuel-rich or

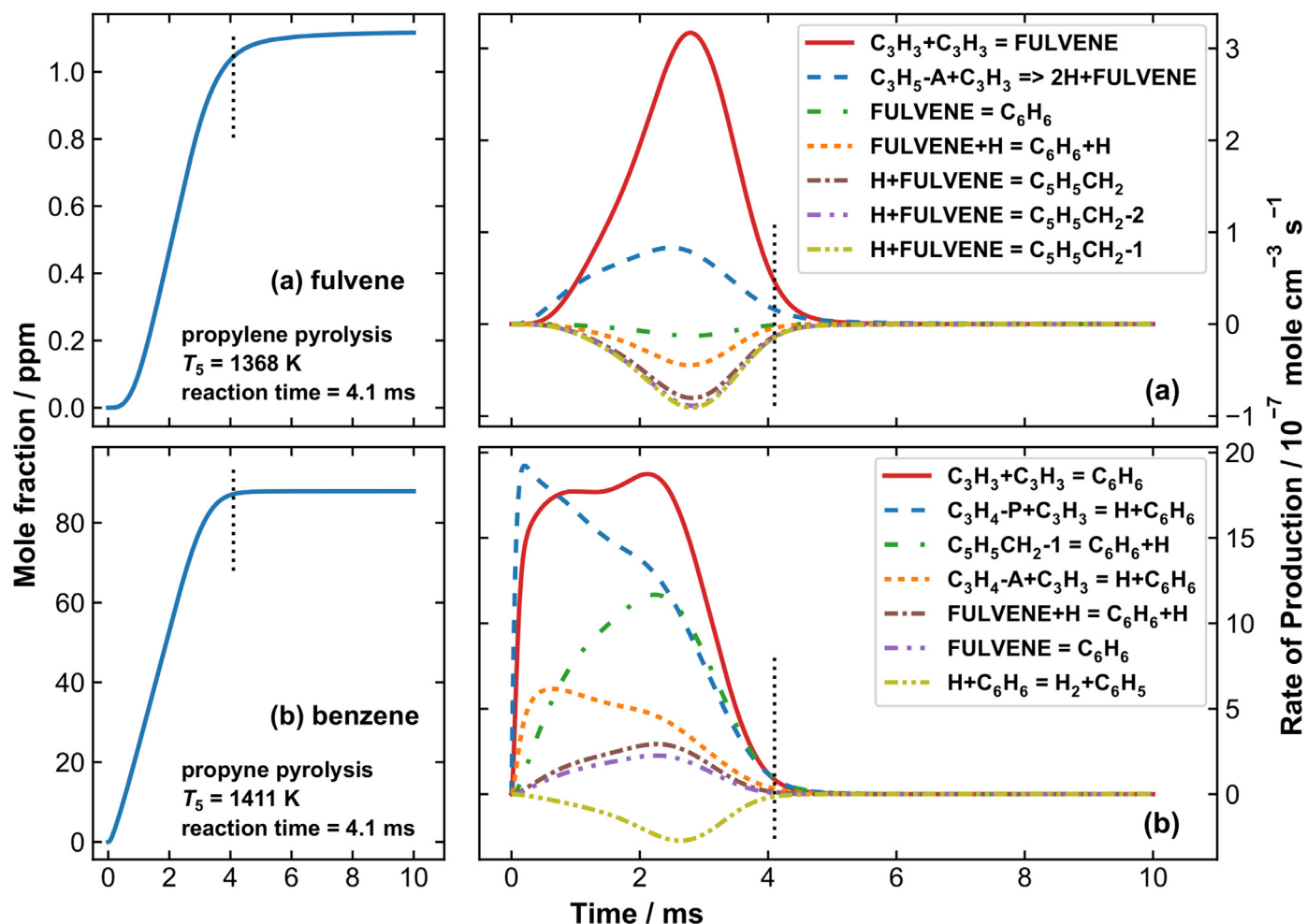


**Fig. 8.** Time-dependent mole fraction profiles (left panel) and rate-of-production analyses (right panel) for (a) fulvene in propylene pyrolysis at  $T_5 = 1368$  K and (b) benzene in propyne pyrolysis at  $T_5 = 1411$  K. Corresponding measured pressure profiles are used in the simulation. The vertical dotted lines indicate the end of the defined reaction time.

pyrolytic conditions. Figure 7 presents the mole fraction profiles of benzene, as well as another important  $\text{C}_6\text{H}_6$  isomer fulvene, which was, however, not detected in our previous experiments of aromatic fuels pyrolysis under similar conditions [30–32]. The measured peak mole fractions of fulvene in propylene and propyne pyrolysis are around 1 ppm and 3 ppm, respectively. Fulvene is formed at lower temperatures than benzene, which suggests its role as a precursor of benzene. It is noteworthy that the ratios between fulvene and benzene peak mole fractions (0.031 and 0.035, respectively) are similar in the two studied cases. Hansen et al. [68] pointed out that a strong linear correlation exists between the mole fractions of these two isomers in low-pressure premixed flames. Such statistical correlations are perhaps also valid among acyclic fuels pyrolysis. The current kinetic model can correctly capture the speciation temperature windows and satisfactorily characterize the peak mole fractions of both isomers, despite a slight overprediction. The peak values of predicted benzene and fulvene mole fractions are not obviously influenced by the used simulation methods. However, by using the measured pressure profiles in the simulation, mole fractions of fulvene in propylene pyrolysis and benzene in propyne pyrolysis are slightly enhanced at moderate temperatures where the species mole fractions are increasing.

To reveal the reasons for the different simulated mole fractions by using the two methods, the time-dependent rate-of-production (ROP) coefficients for fulvene in propylene pyrolysis at  $T_5$  of 1368 K and benzene in propyne pyrolysis at  $T_5$  of 1411 K are shown in

Fig. 8, and the corresponding fulvene and benzene mole fractions that evolve with the time are also illustrated. The results for corresponding isomers (benzene in propylene pyrolysis at  $T_5$  of 1368 K and fulvene in propyne pyrolysis at  $T_5$  of 1411 K) are given in Fig. S14 in the *Supplementary Material*. It is seen that about 10% fulvene is produced during the post-shock quenching, while the formation of benzene is almost completed by the end of the defined reaction time under the analyzed conditions. According to the ROP-analyzed results shown in Fig. 8 and Fig. S14, the  $\text{C}_3\text{H}_3$  self-recombination is one of the primary sources of both benzene and fulvene in the two analyzed cases, and the  $\text{C}_3\text{H}_5\text{-A} + \text{C}_3\text{H}_3$  recombination is also essential towards the formation of fulvene in propylene pyrolysis. Because of a sufficient production of  $\text{C}_3\text{H}_5\text{-A}$ , the  $\text{C}_3\text{H}_5\text{-A} + \text{C}_3\text{H}_3$  channel results in an even higher fulvene production than the  $\text{C}_3\text{H}_3$  self-recombination at the initial stage ( $< 1$  ms) (see Fig. 8). In propyne pyrolysis at  $T_5$  of 1411 K, the formation of benzene proceeds at a high rate at the beginning, given the abundant  $\text{C}_3$  precursors including the fuel  $\text{C}_3\text{H}_4\text{-P}$ , its isomer  $\text{C}_3\text{H}_4\text{-A}$  as well as the fuel radical  $\text{C}_3\text{H}_3$ . Differently, in propylene pyrolysis at 1368 K, the production of fulvene through the  $\text{C}_3 + \text{C}_3$  channels is relatively gradual (see Fig. 8(a)), and as a result, the formation of benzene also starts relatively late (see Fig. S14(a)). This is because the formation of  $\text{C}_3\text{H}_3$  from the fuel requires step-wise dehydrogenation, and thus the reactions involving  $\text{C}_3\text{H}_3$  starts to significantly contribute to fulvene formation at later time points. These reactions continue after the arrival of the quench-

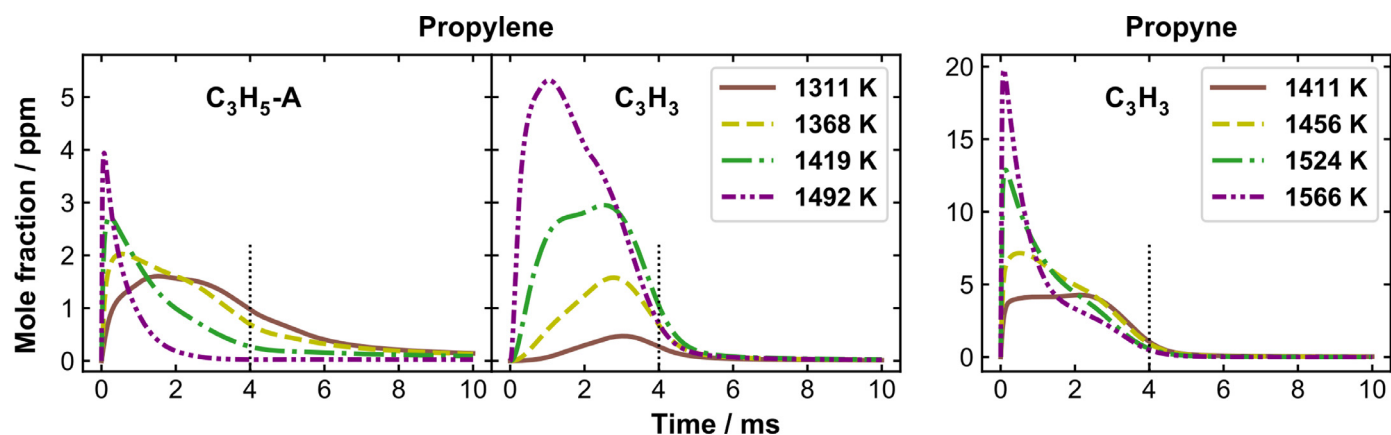


Fig. 9. Simulated time-dependent mole fraction profiles of  $C_3H_5-A$  and  $C_3H_3$  in propylene pyrolysis and  $C_3H_3$  in propyne pyrolysis at specific  $T_5$ s. The vertical dotted lines indicate the end of the reaction time of 4 ms.

ing waves, till 6 ms when the temperature decreases to around 925 K.

Time-dependent mole fraction profiles of  $C_3H_5-A$  and  $C_3H_3$  in propylene pyrolysis and  $C_3H_3$  in propyne pyrolysis at specific  $T_5$ s are shown in Fig. 9. Fuel radicals, *i.e.*  $C_3H_5-A$  in propylene pyrolysis and  $C_3H_3$  in propyne pyrolysis, are formed rapidly, reaching their peak mole fractions in a short time, whereas the consumption spans over a longer time magnitude, particularly for  $C_3H_5-A$  at lower temperatures. The ROP analysis for  $C_3H_5-A$  in propylene pyrolysis at  $T_5 = 1368$  K and at 5 ms is given in Fig. S15 in the Supplementary Material. Due to the relatively low temperature, the self-recombination forming diallyl ( $CH_2=CHCH_2CH_2CH=CH_2$ ) and the recombination with  $CH_3$  producing 1- $C_4H_8$  dominate the consumption of  $C_3H_5-A$  during post-shock quenching. Besides, the recombination with  $C_3H_3$  forming fulvene has a minor contribution (less than 15%), and a small part (about 10%) of the  $C_3H_5-A$  decomposes, responsible for the small amount of  $C_3H_3$  seen after the reaction time of 4 ms.

To understand the three-fold difference between the benzene peak mole fractions in propylene and propyne pyrolysis, sensitivity analyses of benzene are carried out at  $T_5 = 1480$  K, close to the peak temperatures of benzene mole fractions in both cases. The results, as presented in Fig. 10, are distinct in the two cases of propylene and propyne. In propylene pyrolysis, among the most sensitive reactions promoting benzene formation,  $C_3H_3+C_3H_3 = C_6H_6$  is the only one involving benzene, and the rest are the reactions along the dehydrogenation route from  $C_3H_6$  to  $C_3H_3$ . In the case of propyne, the  $C_3H_3$  formation from  $C_3H_4-P$  and  $C_3H_4-A$  decomposition is essential in facilitating benzene formation, besides the  $C_3H_3$  self-recombination and the  $C_3H_4-P+C_3H_3$  reaction. The benzene consumption through hydrogen abstraction has the highest negative sensitivity coefficient. It is seen that in both cases, the addition-elimination reactions of the  $C_3$  fuels ( $C_3H_6/C_3H_4-P$ )+H forming  $CH_3+C_2H_4/C_2H_2$  inhibit the formation of benzene, as it competes with the hydrogen abstraction channel leading to  $C_3$  radicals. The results discussed above suggest that the production of  $C_3H_3$  is the rate-limiting step for  $C_6H_6$  formation in both cases, and this rationalizes the lower benzene mole fraction in propylene pyrolysis, following the lower  $C_3H_3$  production (see Fig. 9).

Monocyclic aromatic hydrocarbons (MAHs) including toluene ( $C_7H_8$ ), phenylacetylene ( $C_6H_5C_2H$ ) and styrene ( $C_6H_5C_2H_3$ ) are observed in both propylene and propyne pyrolysis. The measured mole fractions for these species, as well as simulations with different methods and different models, are presented in Fig. 11.  $C_7H_8$  and  $C_6H_5C_2H$  are more abundant in propyne pyrolysis, while  $C_6H_5C_2H_3$  is measured of similar mole fractions in the two studied cases. The reactions that account for the formation of the MAHs

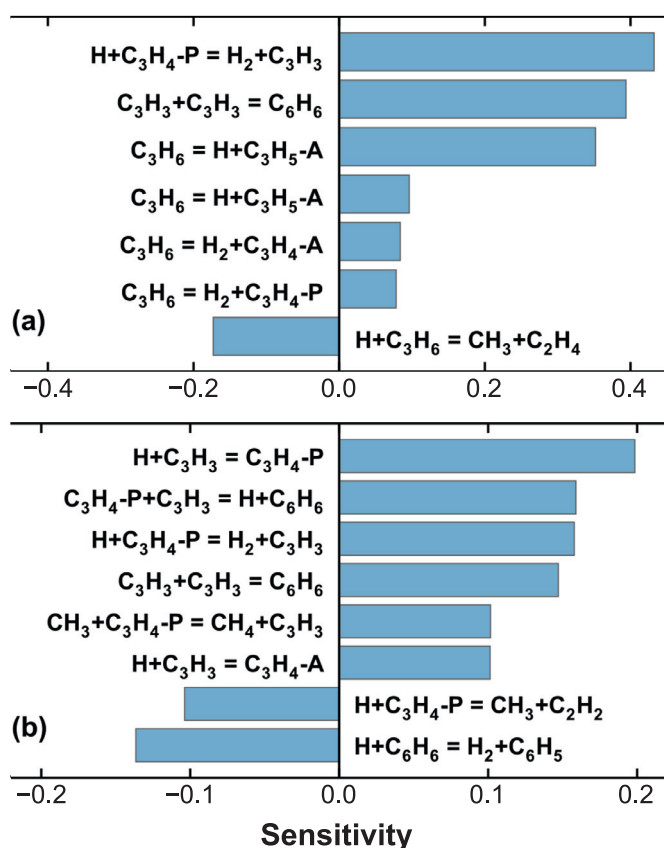
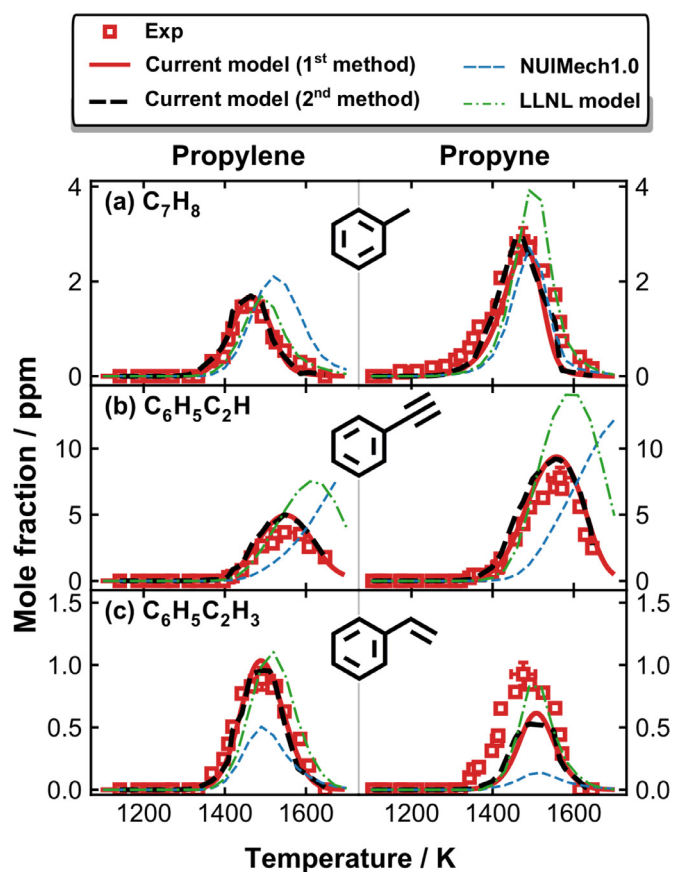


Fig. 10. Sensitivity analysis for  $C_6H_6$  at  $T_5 = 1480$  K in (a) propylene pyrolysis and (b) propyne pyrolysis.

are similar in both propylene and propyne pyrolysis.  $C_7H_8$  has two major sources: the recombination of  $C_3H_3$  with but-2-yn-1-yl radical ( $CH_2C\equiv CCH_3$ ) and the reactions between  $CH_3$  and benzene or phenyl ( $H+C_7H_8 = CH_3+C_6H_6$ ,  $C_7H_8(+M) = CH_3+C_6H_5(+M)$ ), and the later source has higher relative importance at elevated temperatures. The formation of  $C_6H_5C_2H$  and  $C_6H_5C_2H_3$  mostly relies on the reactions of phenyl with acetylene and ethylene, respectively. A higher production of benzene, and thus phenyl, accounts for the more abundant  $C_7H_8$  and  $C_6H_5C_2H$  in propyne pyrolysis. However, the formation of  $C_6H_5C_2H_3$  is limited by the much lower level of  $C_2H_4$  in propyne pyrolysis than that in propylene pyrolysis, as can be noted in Figs. 4 and 5.



**Fig. 11.** Measured (symbols) and simulated (lines) MAHs mole fraction profiles as a function of  $T_5$  in propyne pyrolysis. Thick solid red lines: simulations using the current kinetic model with the constant  $p_5$  of 20 bar and the nominal reaction time of 4 ms; thick dashed black lines: simulations using the current model with measured pressure profiles up to 10 ms; thin dashed blue lines: simulations using the NUIMech1.0 [26] for propylene and [27] for propyne with the constant  $p_5$  of 20 bar and the nominal reaction time of 4 ms; thin dot dashed green lines: simulations using the LLNL PAH model [64] with constant  $p_5$  of 20 bar and the nominal reaction time of 4 ms. (For interpretation of the references to color in this figure legend, the reader is referred to the web version of this article.)

#### 4.3. PAH speciation in propylene and propyne pyrolysis

The current study on the  $C_3$  fuels serves as a fundamental part of our serial works towards a good kinetic understanding of PAH formation from the pyrolysis of practical/surrogate fuels. Thus, it is one of the major intentions to illustrate how PAH species are produced from the species pools of propylene and propyne pyrolysis. Quantitative measurements for PAH species are seldomly reported in literature studies on  $C_3$  fuels pyrolysis, in particular, under high-pressure conditions. In this work, a wealth of two- to four- ring PAHs are identified and quantified in both propylene and propyne pyrolysis. Figure 12 shows the carbon recovery, with and without considering the PAH species, in the two experimental sets. A better carbon balance at elevated temperatures (above 1400 K) is achieved if counting the carbon atoms in PAH species. Note that the PAHs considered here only refer to those identified and quantified in the current experiments. Some peaks, in particular species larger than four-ring, are detected, but cannot be identified or quantified. The carbon balance can be further improved if all gas-phase species are taken into account. Soot particles are formed in the pyrolysis of small  $C_3$  fuels under highly diluted conditions, as carbon deposit is observed on the inner surface of the shock tube after high-temperature experiments. A much better carbon recovery (with a minimum above 90%) is seen in propylene

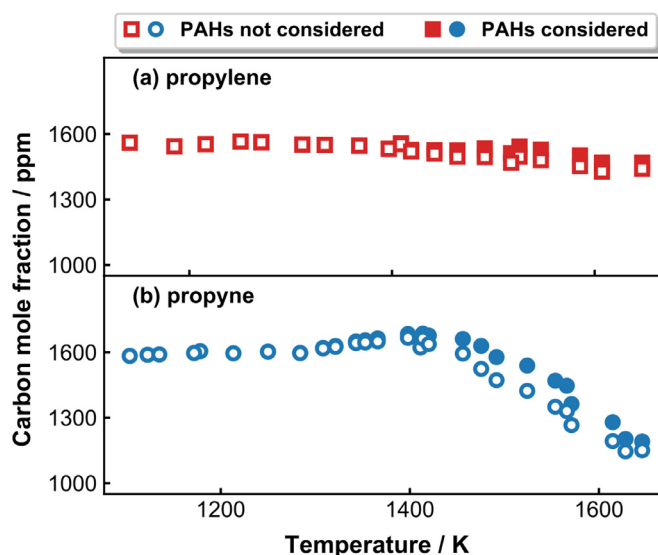


**Fig. 12.** Carbon recovery with and without considering the PAH species in the current experiments of (a) propylene pyrolysis and (b) propyne pyrolysis.

pyrolysis than that in propyne pyrolysis under the same conditions, suggesting a much higher sooting tendency of propyne.

Following the formation of benzene, indene is expected to be one of the first produced PAH species through the  $C_6+C_3$  reactions, given the abundant  $C_3$  radicals and molecules in the species pool. Measured and simulated mole fraction profiles of indene ( $C_9H_8$ ) as well as its non-PAH isomers are shown in Fig. 13. 1-phenylpropyne ( $C_6H_5C\equiv CCH_3$ ,  $C_6H_5C_3H_3P_1$ ) is observed in both cases, whereas phenyl-allene ( $C_6H_5CH=C=CH_2$ ,  $C_6H_5C_3H_3A$ ) is only detected in propyne pyrolysis. The current kinetic model can satisfactorily predict the measured mole fraction distributions of the  $C_9H_8$  isomers. This is mainly owing to the inclusion of the theoretical rate coefficients reported in a series of works on  $C_6+C_3$  reactions by Mebel and coworkers [9–11].  $C_9H_8$  is much more abundant than  $C_6H_5C_3H_3P_1$  and  $C_6H_5C_3H_3A$ , though in the  $C_6+C_3$  reaction systems, the channels leading to substituted benzene compounds take comparable or even higher branching ratios than the one forming indene, according to the theoretical results [9]. In propyne pyrolysis, the three isomers start to form at similar temperatures, but the mole fractions of the non-PAH species peak at lower temperatures than indene. This suggests that the consumption of  $C_6H_5C_3H_3P_1$  and  $C_6H_5C_3H_3A$  contributes to the formation of  $C_9H_8$  at elevated temperatures. 3-phenyl-propyne ( $C_6H_5CH_2C\equiv CH$ ,  $C_6H_5C_3H_3P_3$ )+H is predicted to be a major bimolecular product of  $C_6H_5+C_3H_4-A$  reactions [9], but  $C_6H_5C_3H_3P_3$  is not detected in the current experiments. The simulated peak mole fractions of  $C_6H_5C_3H_3P_3$  (0.01 ppm and 0.05 ppm in propylene and propyne pyrolysis, respectively) are lower than those of  $C_6H_5C_3H_3P_1$  and  $C_6H_5C_3H_3A$ .  $C_6H_5C_3H_3P_1$  is mainly formed through the molecule+radical reactions of  $C_3H_4-P+C_6H_5$  and  $C_6H_5C_2H+CH_3$ , and the later channel is predominant at elevated temperatures. Regarding the formation of  $C_6H_5C_3H_3A$ , the radical+radical reaction  $C_6H_5+C_3H_3$  is the major source, and the reaction  $C_3H_4-P+C_6H_5 = C_6H_5C_3H_3A+H$  also has contributions in propyne pyrolysis at moderate temperatures (1300–1400 K for instance).

Back to the more concerned PAH isomer indene ( $C_9H_8$ ), the main formation pathways are shown in Fig. 14, which also presents the reaction schemes responsible for the production of other major PAH species measured in this work. These reaction pathways are mapped out based on ROP analyses at 1550 K, where most PAH species have considerable mole fractions, and the relevant details will be discussed later in this section. As mentioned above,  $C_9H_8$



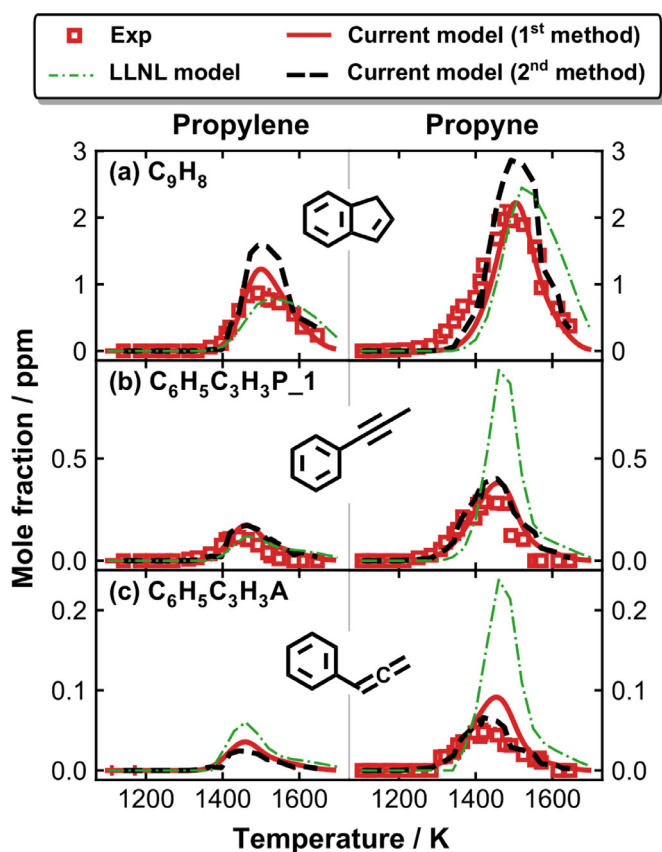


**Fig. 13.** Measured (symbols) and simulated (lines) mole fraction profiles for  $C_9H_8$  isomers as a function of  $T_5$  in propyne pyrolysis. Thick solid red lines: simulations using the current kinetic model with the constant  $p_5$  of 20 bar and the nominal reaction time of 4 ms; thick dashed black lines: simulations using the current model with measured pressure profiles up to 10 ms; thin dot dashed green lines: simulations using the LLNL PAH model [64] with constant  $p_5$  of 20 bar and the nominal reaction time of 4 ms.

formation mainly depends on the consumption of  $C_6H_5C_3H_3P_1$  and  $C_6H_5C_3H_3A$ , and the benzyl+acetylene ( $C_7H_7+C_2H_2$ ) channel also has a minor contribution. It can be noted that the formation of  $C_9H_8$  carries on during the post-shock quenching (see Fig. 13(a)). This is partly due to the isomerization of  $C_6H_5C_3H_3A$ , for which the simulated mole fractions decrease when using the measure pressure profiles up to 10 ms (see Fig. 13(c)). Besides, a part of indenyl ( $C_9H_7$ ) radicals converts back to  $C_9H_8$  by recombining with H atoms, due to the decreasing temperature after the reaction time of 4 ms.

$C_9H_7$  is an important species in the shown reaction pathways (see Fig. 14), as it is related to the formation of some other PAHs, including naphthalene ( $C_{10}H_8$ ) and acenaphthalene ( $C_{12}H_8$ ), the most abundant ones detected in the current work. The mole fraction profiles of naphthalene ( $C_{10}H_8$ ) and its isomer benzofulvene ( $C_9H_6CH_2$ ) are shown in Fig. 15. This couple of isomers is expected to share some similarities with the benzene-fulvene isomer pair. Regarding the structural features, naphthalene and benzofulvene have one more aromatic ring in comparison to benzene and fulvene, respectively. In terms of the speciation behaviors, benzofulvene has a lower temperature window and a smaller peak mole fraction than naphthalene. Moreover, benzofulvene is a vital precursor of naphthalene (see Fig. 14), and the isomerization of a methylene ( $CH_2=$ ) substituted cyclopenta-ring to an aromatic ring is similar to the case of fulvene to benzene conversion. According to the ROP-analyzed results, the formation of both benzofulvene and naphthalene relies on three major channels: i) the con-

sumption of methyl-indene radical ( $C_9H_7CH_2$ ) following the production of methyl-indene ( $C_9H_7CH_3$ ) through  $C_9H_7+CH_3$  recombination; ii) the recombination between fulvenallyl ( $C_7H_5$ ) and  $C_3H_3$ . (To point out,  $C_7H_5$  mainly comes from benzyl ( $C_7H_7$ ) decomposition and the  $C_3H_3+C_4H_2$  recombination); iii) the hydrogen abstraction acetylene addition (HACA) route through phenylacetylene radical ( $C_6H_4C_2H$ ) with  $C_2H_2$  leading to benzofulvenyl ( $C_9H_6CH$ ) and naphthyl ( $C_{10}H_7$ ) radicals which convert to benzofulvene and naphthalene, respectively, by recombination with a hydrogen atom. The relative importance of the mentioned channels varies with the temperature, and the third one has relatively higher contribution at elevated temperatures. Towards the formation of  $C_{10}$  PAHs, besides the above mentioned  $C_9+C_1$ ,  $C_7+C_3$  and  $C_8+C_2$  channels, the  $C_6+C_4$  and  $C_5+C_5$  are also potential sources, as suggested in literature [9,69–71], and relevant reactions are considered in the kinetic model. Under the currently investigated conditions, a part of naphthyl radical ( $C_{10}H_7$ ) is formed through  $C_6H_5+C_4H_2$ , whereas the  $C_5+C_5$  reactions, such as the cyclopentadienyl ( $C_5H_5$ ) self-recombination, does not have obvious contributions.

Figure 16 displays the mole fraction profiles of  $C_{10}$ – $C_{13}$  PAHs including 1-methyl-indene ( $C_9H_7CH_3$ ), 1-methyl naphthalene ( $C_{10}H_7CH_3$ ), biphenyl ( $C_6H_5C_6H_5$ ), acenaphthalene ( $C_{12}H_8$ ), 1-ethynyl-naphthalene ( $C_{10}H_7C_2H$ ) and fluorene ( $C_{13}H_{10}$ ). All shown PAHs have higher mole fractions in propyne pyrolysis than in propylene pyrolysis. The measurements can be satisfactorily predicted with the current kinetic model using the measured pressure profiles (the second simulation method). As mentioned above,  $C_9H_7CH_3$  is an important precursor for the naphthalene-benzofulvene isomer pair. The majority of  $C_9H_7CH_3$  is formed during the post-shock quenching, mainly through the  $C_9H_7+CH_3$  recombination.  $C_6H_5C_6H_5$  mainly comes from the reaction between benzene and phenyl ( $C_6H_6+C_6H_5 = C_6H_5C_6H_5+H$ ). Due to the different benzene/phenyl mole fractions in propylene and propyne, the difference in biphenyl mole fractions in the two cases are remarkable: the peak  $C_6H_5C_6H_5$  mole fraction in propyne pyrolysis is about 6 times higher than that in propylene pyrolysis, while for other PAHs, a ratio of 2–2.5 is seen between the peak mole fractions in the two cases. A minor contribution to  $C_6H_5C_6H_5$  formation comes from the reaction between phenyl-propargyl radical ( $C_6H_5C_3H_2$ ,  $C_6H_5C\equiv CCH_2$ ) and  $C_3H_3$ , similar to benzene formation through  $C_3H_3$  self-recombination. The formation of the rest PAHs shown in Fig. 16 involves the participation of naphthyl ( $C_{10}H_7$ ): the  $C_{10}H_7+CH_3$  recombination is the predominant source of  $C_{10}H_7CH_3$ ; the addition-elimination  $C_{10}H_7+C_2H_2 = C_{10}H_7C_2H+H$  controls the formation of  $C_{10}H_7C_2H$  and accounts for a small part (12% at 1550 K) of  $C_{12}H_8$  production (see Fig. 14);  $C_{10}H_7+C_3H_4-P$  is an essential pathway leading to  $C_{13}H_{10}$  (not shown in Fig. 14).  $C_{12}H_8$  is an abundant PAH in both propylene and propyne pyrolysis, and according to the ROP analysis, it is mainly produced through the  $C_9H_7+C_3H_3$  pathway proposed in [72]. Besides, a minor channel via the step-wise isomerization starting from the biphenyl radical ( $C_6H_5C_6H_4$ ,  $C_{12}H_9$ ) [60,73] contributes to around 5%  $C_{12}H_8$  formation at 1550 K.

Four different  $C_{14}H_{10}$  species are identified and quantified in both propylene and propyne pyrolysis, including the dominant phenanthrene ( $PC_{14}H_{10}$ ), and its isomers, 9-methylene-fluorene ( $C_{13}H_8CH_2$ ), anthracene ( $AC_{14}H_{10}$ ) and diphenylacetylene ( $C_6H_5CCC_6H_5$ ). Corresponding mole fraction measurements, together with the simulated results, are given in Fig. 17. It can be seen that, compared to the LLNL PAH model, the current model can better characterize the measured mole fraction distribution, in particular for the minor isomers  $C_6H_5CCC_6H_5$  and  $C_{13}H_8CH_2$ . According to the ROP analyses at 1550 K using the current model, the addition-elimination reactions of  $C_6H_5+C_6H_5C_2H$  result in  $C_{13}H_8CH_2$  and  $C_6H_5CCC_6H_5$ , both of which further isomer-



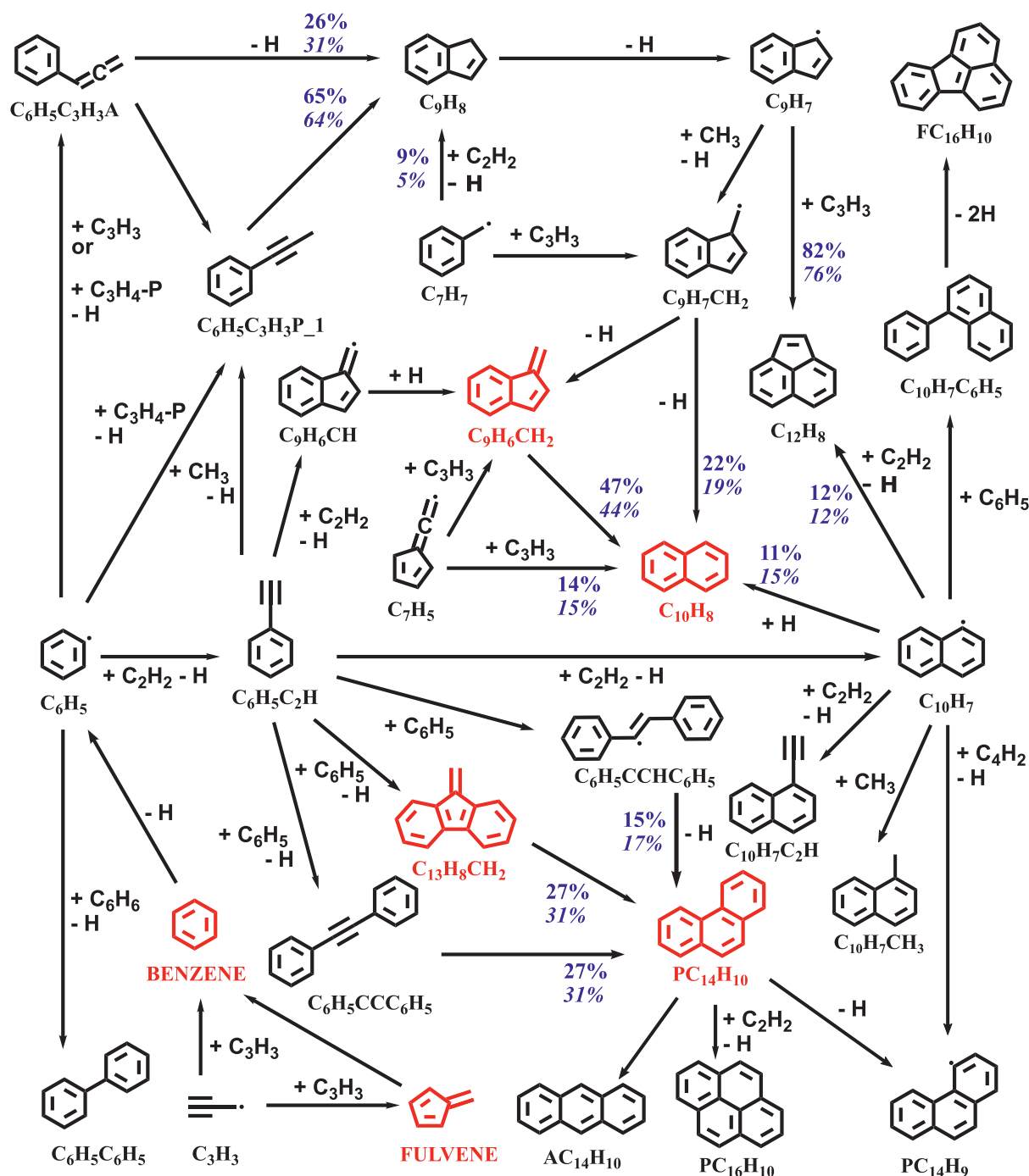


**Fig. 14.** Major PAH formation pathways in propylene and propyne pyrolysis based on ROP analyses at 1550 K. The percentage numbers (normal font: in propylene pyrolysis; italic font: in propyne pyrolysis) represent the contributions of corresponding reactions to the formation of important PAHs. The highlighted species are the one- to three-ring aromatics (benzene, naphthalene, phenanthrene) and their cyclopenta-ring isomers (fulvene, benzofulvene and 9-methylene-fluorene).

ize to  $PC_{14}H_{10}$  (see Fig. 14). Differently, the LLNL model predicts that the formation of  $PC_{14}H_{10}$  mainly relies on the HACA route through  $C_{12}H_9$  (biphenyl radical)+ $C_2H_2$  and the dehydrogenation of a  $C_{14}H_{11}$  radical formed from  $C_6H_5$  addition to  $C_6H_5C_2H$ , while the  $C_{13}H_8CH_2$  and  $C_6H_5CCC_6H_5$  isomers are not involved in relevant reaction pathways. The  $C_6H_5+C_6H_5C_2H$  addition-elimination reactions are found as important channels leading to fuel consumption and the formation of  $C_{14}H_{10}$  products ( $C_6H_5CCC_6H_5$ ,  $C_{13}H_8CH_2$ ,  $PC_{14}H_{10}$ ) in  $C_6H_5C_2H$  pyrolysis in our previous work [31]. The involved pathways and corresponding rate coefficients,

mostly from a theoretical study by Matsugi and Miyoshi [71], have been validated with the quantitative measurements in [31]. The inclusion of the above-mentioned reactions, which are however missing from the LLNL PAH model, results in a better prediction for the relevant  $C_{14}H_{10}$  PAHs using the current model. The more abundant  $C_6H_5$  and  $C_6H_5C_2H$  account for the much higher (around 5 times) peak mole fractions of  $C_{13}H_8CH_2$  and  $C_6H_5CCC_6H_5$  in propyne pyrolysis, in comparison to the case of propylene pyrolysis. However, the  $PC_{14}H_{10}$  peak mole fraction in propylene pyrolysis is about half of that in propyne pyrolysis.

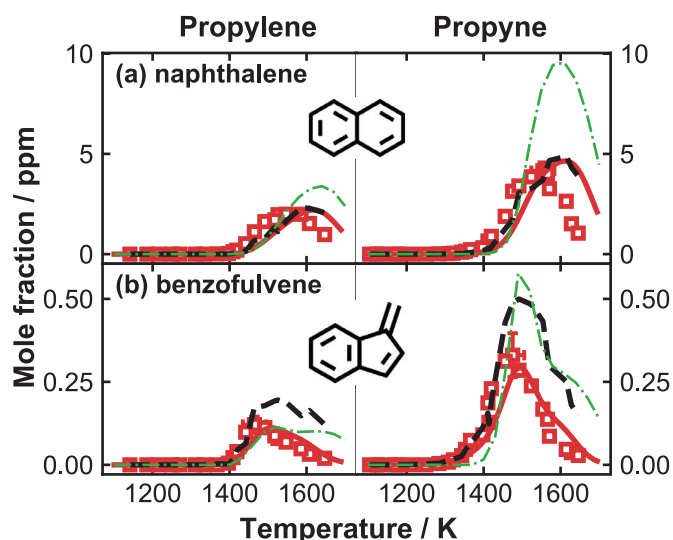


**Fig. 15.** Measured (symbols) and simulated (lines) naphthalene and benzofulvene mole fraction profiles as a function of  $T_5$  in propyne pyrolysis. Thick solid red lines: simulations using the current kinetic model with the constant  $p_5$  of 20 bar and the nominal reaction time of 4 ms; thick dashed black lines: simulations using the current model with measured pressure profiles up to 10 ms; thin dot dashed green lines: simulations using the LLNL PAH model [64] with constant  $p_5$  of 20 bar and the nominal reaction time of 4 ms. (For interpretation of the references to color in this figure legend, the reader is referred to the web version of this article.)

This is because the isomerization of  $C_{13}H_8CH_2$  and  $C_6H_5CCC_6H_5$  to  $PC_{14}H_{10}$  ( $C_{13}H_8CH_2/C_6H_5CCC_6H_5 + H = PC_{14}H_{10} + H$ ) requires the participation of H atoms, and a larger amount of H atoms exists

in the reaction system of propylene decomposition. Similar to the above discussed benzene-fulvene and naphthalene-benzofulvene isomer pairs, the aromatic ring formation through the isomerization of its cyclopenta-ring counterpart is also seen in the case of  $C_{13}H_8CH_2 \rightarrow PC_{14}H_{10}$  (see Fig. 14). The methylene substituted cyclopenta-ring species are important precursors leading to aromatic ring growth in the current studied cases. Such structures are attainable through  $CH_3$  addition reactions, *i.e.* formed as intermediates along the methyl addition/cyclization (MAC) [74] routes, which are found as important PAH growth pathways under combustion related conditions [75–77]. The current model can well predict the speciation of  $PC_{14}H_{10}$ ,  $C_{13}H_8CH_2$  and  $C_6H_5CCC_6H_5$ , while improvements are necessary to better characterize the mole fraction profiles of  $AC_{14}H_{10}$ , particularly in propylene pyrolysis. The model predicts higher peak temperatures for  $AC_{14}H_{10}$  than the experiments in both studied cases. A likely explanation is that there are reactions, other than the  $PC_{14}H_{10}$  isomerization, which lead to  $AC_{14}H_{10}$  formation at lower temperatures, missing from the current model. The  $AC_{14}H_{10}$  formation chemistry, as is not well-established, merits future investigations through theoretical and experimental methods. Based on the above discussion, a cyclopenta-ring isomer, 1-methylene-1H-cyclopenta[b]naphthalene might be a potential precursor of  $AC_{14}H_{10}$ .

Mole fraction distributions for the  $C_{16}H_{10}$  isomers, fluoranthene ( $FC_{16}H_{10}$ ) and pyrene ( $PC_{16}H_{10}$ ), and another  $C_{16}$  PAH 1-phenyl-naphthalene ( $C_{10}H_7C_6H_5$ ) are shown in Fig. 18. All  $C_{16}$  PAHs are present in trace amounts, with peak mole fractions below 0.1 ppm. The isomers,  $FC_{16}H_{10}$  and  $PC_{16}H_{10}$ , are formed through different channels according to the current kinetic model.  $FC_{16}H_{10}$  is mainly formed through the dehydrogenation of  $C_{10}H_7C_6H_5$  follow-

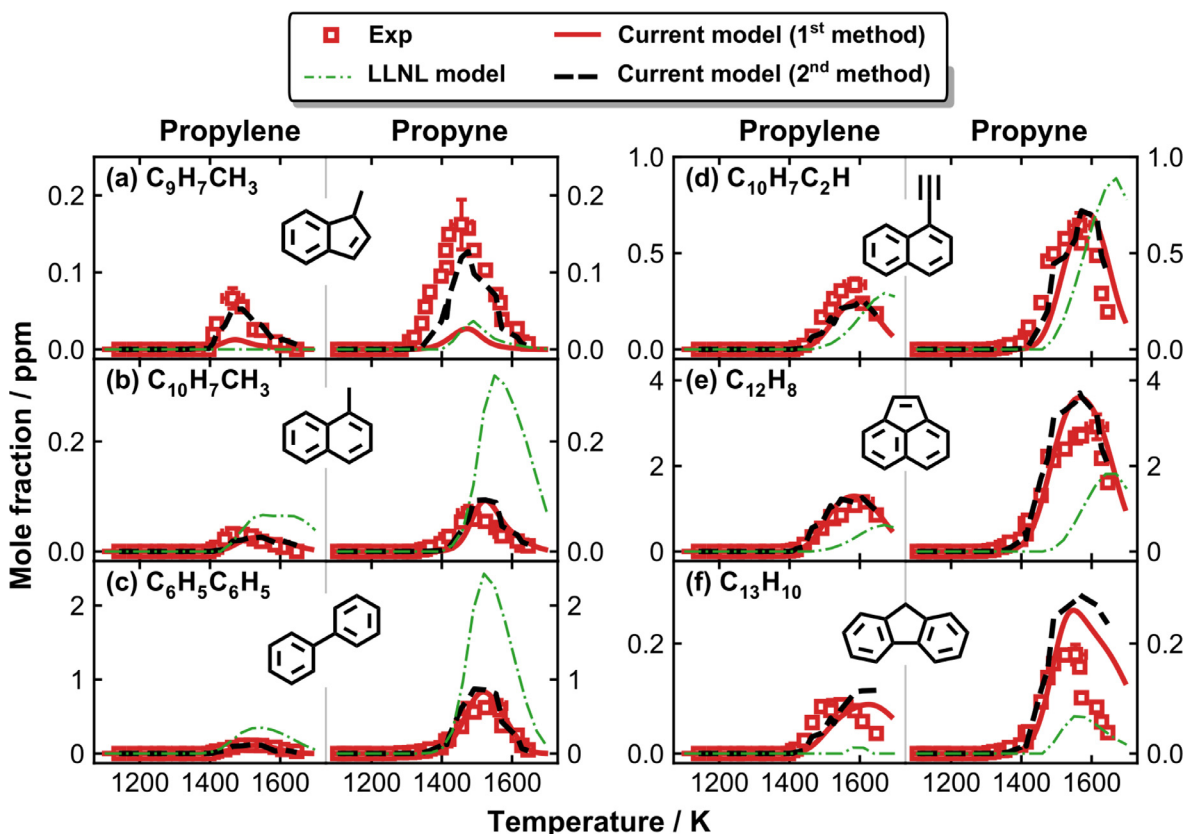


**Fig. 16.** Measured (symbols) and simulated (lines) mole fraction profiles for specific  $C_{10}$ – $C_{13}$  PAH species as a function of  $T_5$  in propyne pyrolysis. Thick solid red lines: simulations using the current kinetic model with the constant  $p_5$  of 20 bar and the nominal reaction time of 4 ms; thick dashed black lines: simulations using the current model with measured pressure profiles up to 10 ms; thin dot dashed green lines: simulations using the LLNL PAH model [64] with constant  $p_5$  of 20 bar and the nominal reaction time of 4 ms. (For interpretation of the references to color in this figure legend, the reader is referred to the web version of this article.)

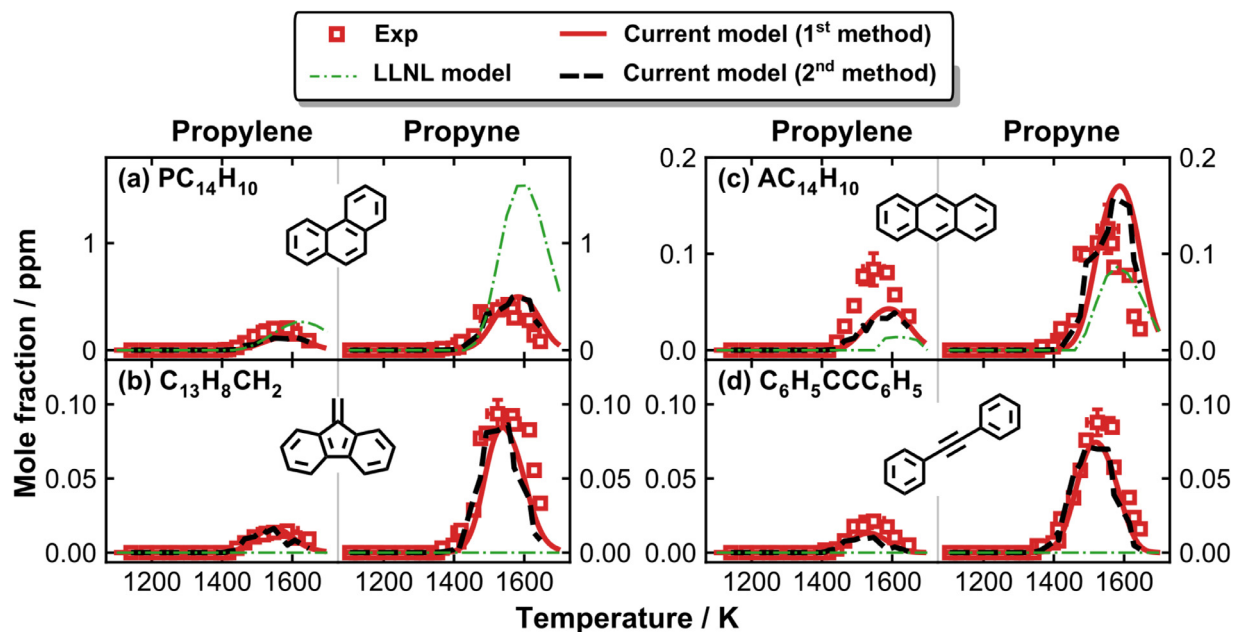


**Fig. 17.** Measured (symbols) and simulated (lines) mole fraction profiles for  $C_{14}H_{10}$  isomers as a function of  $T_5$  in propyne pyrolysis. Thick solid red lines: simulations using the current kinetic model with the constant  $p_5$  of 20 bar and the nominal reaction time of 4 ms; thick dashed black lines: simulations using the current model with measured pressure profiles up to 10 ms; thin dot dashed green lines: simulations using the LLNL PAH model [64] with constant  $p_5$  of 20 bar and the nominal reaction time of 4 ms. (For interpretation of the references to color in this figure legend, the reader is referred to the web version of this article.)

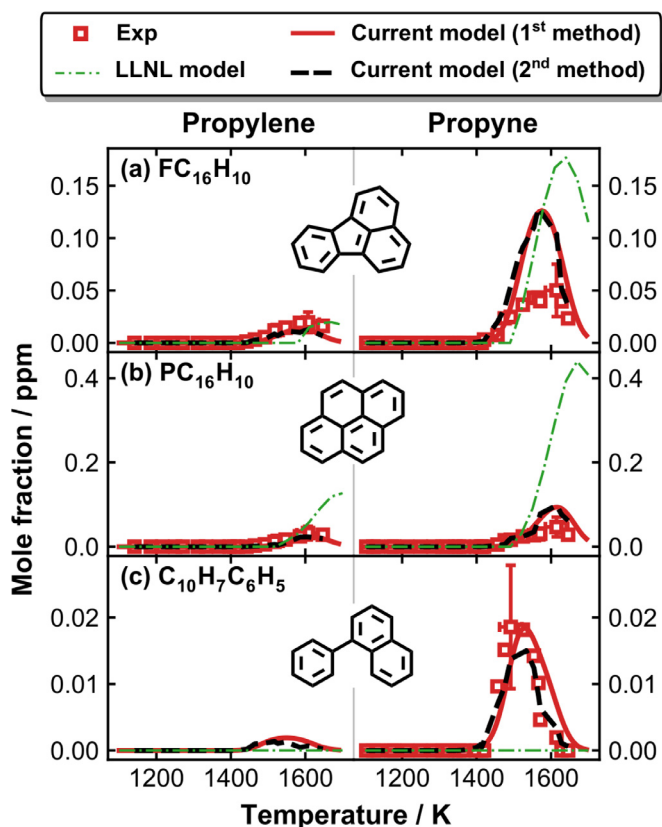


**Fig. 18.** Measured (symbols) and simulated (lines) fluoranthene ( $FC_{16}H_{10}$ ), pyrene ( $C_{16}H_{10}$ ) and 1-phenyl-naphthalene ( $C_{10}H_7C_6H_5$ ) mole fraction profiles as a function of  $T_5$  in propyne pyrolysis. Thick solid red lines: simulations using the current kinetic model with the constant  $p_5$  of 20 bar and the nominal reaction time of 4 ms; thick dashed black lines: simulations using the current model with measured pressure profiles up to 10 ms; thin dot dashed green lines: simulations using the LLNL PAH model [64] with constant  $p_5$  of 20 bar and the nominal reaction time of 4 ms. (For interpretation of the references to color in this figure legend, the reader is referred to the web version of this article.)

ing the reaction between  $C_{10}H_7$  and  $C_6H_6$ ; while the production of  $C_{16}H_{10}$  relies on the HACA mechanism of phenanthryl radical ( $PC_{14}H_9$ ) +  $C_2H_2$ . As a precursor of  $FC_{16}H_{10}$ ,  $C_{10}H_7C_6H_5$  has a relatively lower peak temperature, and it is under the detection limit of 0.01 ppm in propylene pyrolysis. Such observations can be captured by the current kinetic model.

## 5. Conclusions

In this work, we go back to the fundamental  $C_3$  fuels to examine the formation of the first aromatic ring, benzene, up to two- to four- ring PAH compounds from the species pool of propylene and propyne decomposition. Shock tube pyrolysis experiments are conducted with highly argon-diluted mixtures containing 500 ppm of propylene or propyne at a nominal pressure of 20 bar over a temperature range of 1050–1650 K. Post-shock mixtures are sampled and analyzed via GC/GC-MS techniques, yielding species mole fraction profiles as a function of the post-shock temperature  $T_5$ . Updates, mainly regarding the reactions involving  $C_3$  molecules and radicals, are made in our on-going PAH kinetic model, which shows satisfactory predictive performances for the speciation measurements obtained in the current work as well those reported in literature studies on propylene and propyne pyrolysis. Propylene and propyne show distinct decomposition reactivity, and the consumption of propyne follows a unique curve because of the characteristic isomerization reaction to allene. Propyne is among the propylene pyrolysis products, and thus all small hydrocarbons produced from propyne consumption are also present in the species pool of propylene pyrolysis. Fulvene, which was not detected in previous pyrolysis experiments of aromatic fuels, is observed in non-negligible amounts and found as one of the major benzene precursors in propylene and propyne pyrolysis. The formation of benzene relies on  $C_3+C_3$  reactions, more specifically, the self-combination of propargyl and the propargyl+propyne reaction; besides, fulvene is also an important benzene precursor. The production of propargyl through fuel dehydrogenation steps is analyzed to be the rate-limiting step in benzene formation in the pyrolysis of both  $C_3$  fuels, which rationalizes the higher benzene mole fractions in propyne

pyrolysis. Consequently, propyne shows a much higher PAH formation tendency than propylene, given the essential role of the “first aromatic ring” production. Although the PAHs have distinct abundance in propylene and propyne pyrolysis, the major PAH formation pathways are similar in the two cases. Indene is formed via the interactions between benzene (or phenyl) and the C<sub>3</sub> species including the fuels and fuel radicals. By reacting with the abundant methyl and propargyl, indenyl plays an important role in the formation of naphthalene and acenaphthalene, the most abundant PAHs measured in the experiments. The methylene substituted cyclopenta-ring species are found as important precursors leading to the growth of aromatic ring, more specifically, through direct or H-assisted isomerization reactions. Beyond benzene and phenyl, C<sub>7</sub> radicals such as benzyl and fulvenallyl, despite their limited quantities, are also found to contribute to the PAH formation through reactions with C<sub>2</sub>–C<sub>3</sub> species. Different from the case of benzene pyrolysis, C<sub>3</sub> species, in particular, the resonantly stabilized radicals propargyl and allyl have considerable mole fractions in propylene and propyne pyrolysis. The interplays between the C<sub>3</sub> radicals and the mentioned aromatic species have great potential to induce larger PAHs, and such topics will be further investigated in our future studies.

### Declaration of Competing Interest

The authors declare that they have no known competing financial interests or personal relationships that could have appeared to influence the work reported in this paper.

### Acknowledgments

This project has received funding from the [European Research Council](#) (ERC) under the European Union’s Horizon 2020 research and innovation program (grant agreement No. [756785](#)).

### Supplementary materials

Supplementary material associated with this article can be found, in the online version, at doi:[10.1016/j.combustflame.2021.111485](https://doi.org/10.1016/j.combustflame.2021.111485).

### References

- J.A. Miller, S.J. Klippenstein, The recombination of propargyl radicals and other reactions on a C<sub>6</sub>H<sub>6</sub> potential, *J. Phys. Chem. A* 107 (2003) 7783–7799.
- N. Hansen, J.A. Miller, P.R. Westmoreland, T. Kasper, K. Kohse-Höinghaus, J. Wang, T.A. Cool, Isomer-specific combustion chemistry in allene and propyne flames, *Combust. Flame* 156 (2009) 2153–2164.
- J.A. Miller, S.J. Klippenstein, The recombination of propargyl radicals: solving the master equation, *J. Phys. Chem. A* 105 (2001) 7254–7266.
- C.J. Pope, J.A. Miller, Exploring old and new benzene formation pathways in low-pressure premixed flames of aliphatic fuels, *Proc. Combust. Inst.* 28 (2000) 1519–1527.
- N. Hansen, J.A. Miller, C.A. Taatjes, J. Wang, T.A. Cool, M.E. Law, P.R. Westmoreland, Photoionization mass spectrometric studies and modeling of fuel-rich allene and propyne flames, *Proc. Combust. Inst.* 31 (2007) 1157–1164.
- J.A. Miller, C.F. Melius, Kinetic and thermodynamic issues in the formation of aromatic compounds in flames of aliphatic fuels, *Combust. Flame* 91 (1992) 21–39.
- A. Raj, M.J. Al Rashidi, S.H. Chung, S.M. Sarathy, PAH growth initiated by propargyl addition: mechanism development and computational kinetics, *J. Phys. Chem. A* 118 (2014) 2865–2885.
- A.M. Mebel, Y. Georgievskii, A.W. Jasper, S.J. Klippenstein, Pressure-dependent rate constants for PAH growth: formation of indene and its conversion to naphthalene, *Faraday Discuss.* 195 (2017) 637–670.
- A.M. Mebel, A. Landera, R.I. Kaiser, Formation mechanisms of naphthalene and indene: from the interstellar medium to combustion flames, *J. Phys. Chem. A* 121 (2017) 901–926.
- A.N. Morozov, A.M. Mebel, Theoretical Study of the Reaction Mechanism and Kinetics of the Phenyl+ Allyl and Related Benzyl+ Vinyl Associations, *J. Phys. Chem. A* 123 (2019) 1720–1729.
- A.N. Morozov, A.M. Mebel, Theoretical study of the reaction mechanism and kinetics of the phenyl+ propargyl association, *Phys. Chem. Chem. Phys.* 22 (2020) 6868–6880.
- J.N. Bradley, K.O. West, Single-pulse shock tube studies of hydrocarbon pyrolysis. Part 4.—Isomerization of allene to methylacetylene, *J. Chem. Soc. Faraday Trans.1* 71 (1975) 967–971.
- A. Burcat, Cracking of propylene in a shock tube, *Fuel* 54 (1975) 87–93.
- A. Lifshitz, M. Frenklach, A. Burcat, Structural isomerization allene-propyne. Studies with a single pulse shock tube, *J. Phys. Chem.* 79 (1975) 1148–1152.
- J. Kiefer, M. Al-Alami, K. Budach, A shock tube, laser-schlieren study of propene pyrolysis at high temperatures, *J. Phys. Chem.* 86 (1982) 808–813.
- T. Kakumoto, T. Ushirogouchi, K. Saito, A. Imamura, Isomerization of allene-propyne in shock waves and ab initio calculations, *J. Phys. Chem.* 91 (1987) 183–189.
- Y. Hidaka, T. Nakamura, A. Miyauchi, T. Shiraiishi, H. Kawano, Thermal decomposition of propyne and allene in shock waves, *Int. J. Chem. Kinet.* 21 (1989) 643–666.
- V.S. Rao, G.B. Skinner, Study of the high-temperature pyrolysis of propene by determination of H and D atoms formed from partially deuterated propenes heated behind shock waves, *J. Phys. Chem.* 93 (1989) 1869–1876.
- Y. Hidaka, T. Nakamura, H. Tanaka, A. Jinno, H. Kawano, T. Higashihara, Shock tube and modeling study of propene pyrolysis, *Int. J. Chem. Kinet.* 24 (1992) 761–780.
- S. Davis, C. Law, H. Wang, Propene pyrolysis and oxidation kinetics in a flow reactor and laminar flames, *Combust. Flame* 119 (1999) 375–399.
- S.G. Davis, C.K. Law, H. Wang, Propyne pyrolysis in a flow reactor: an experimental, RRKM, and detailed kinetic modeling study, *J. Phys. Chem. A* 103 (1999) 5889–5899.
- K. Norinaga, V.M. Janardhanan, O. Deutschmann, Detailed chemical kinetic modeling of pyrolysis of ethylene, acetylene, and propylene at 1073–1373K with a plug-flow reactor model, *Int. J. Chem. Kinet.* 40 (2008) 199–208.
- T. Bentz, B.R. Giri, H. Hippler, M. Olzmann, F. Striebel, M. Szöri, Reaction of hydrogen atoms with propyne at high temperatures: an experimental and theoretical study, *J. Phys. Chem. A* 111 (2007) 3812–3818.
- I. Weber, L. Golka, M. Olzmann, Thermal decomposition of propene: a shock-tube/H-ARAS and modeling study, *Proc. Combust. Inst.* 36 (2017) 299–306.
- K. Wang, S.M. Villano, A.M. Dean, Fundamentally-based kinetic model for propene pyrolysis, *Combust. Flame* 162 (2015) 4456–4470.
- S.S. Nagaraja, J. Liang, S. Dong, S. Panigrahy, A. Sahu, G. Kukkadapu, S.W. Wagnon, W.J. Pitz, H.J. Curran, A hierarchical single-pulse shock tube pyrolysis study of C<sub>2</sub>–C<sub>6</sub> 1-alkenes, *Combust. Flame* 219 (2020) 456–466.
- S. Panigrahy, J. Liang, S.S. Nagaraja, Z. Zuo, G. Kim, S. Dong, G. Kukkadapu, W.J. Pitz, S.S. Vasu, H.J. Curran, A comprehensive experimental and improved kinetic modeling study on the pyrolysis and oxidation of propyne, *Proc. Combust. Inst.* 38 (2021) 479–488.
- A. Kallend, J. Purnell, B. Shurlock, The pyrolysis of propylene, *Proc. R. Soc. Lond. Ser. A Math. Phys. Sci.* 300 (1967) 120–139.
- H. Wang, X. You, A.V. Joshi, S.G. Davis, A. Laskin, F. Egolfopoulos, C.K. Law, USC Mech Version II. High-Temperature Combustion Reaction Model of H<sub>2</sub>/CO/C<sub>1</sub>–C<sub>4</sub> Compounds. [http://ignis.usc.edu/USC\\_Mech\\_II.htm](http://ignis.usc.edu/USC_Mech_II.htm), May 2007.
- W. Sun, A. Hamadi, S. Abid, N. Chaumeix, A. Comandini, Probing PAH formation chemical kinetics from benzene and toluene pyrolysis in a single-pulse shock tube, *Proc. Combust. Inst.* 38 (2021) 891–900.
- W. Sun, A. Hamadi, S. Abid, N. Chaumeix, A. Comandini, An experimental and kinetic modeling study of phenylacetylene decomposition and the reactions with acetylene/ethylene under shock tube pyrolysis conditions, *Combust. Flame* 220 (2020) 257–271.
- W. Sun, A. Hamadi, S. Abid, N. Chaumeix, A. Comandini, A comparative kinetic study of C<sub>8</sub>–C<sub>10</sub> linear alkylbenzenes pyrolysis in a single-pulse shock tube, *Combust. Flame* 221 (2020) 136–149.
- W. Sun, A. Hamadi, S. Abid, N. Chaumeix, A. Comandini, Detailed experimental and kinetic modeling study of toluene/C<sub>2</sub> pyrolysis in a single-pulse shock tube, *Combust. Flame* 226 (2021) 129–142.
- W. Pejpichestakul, E. Ranzi, M. Pelucchi, A. Frassoldati, A. Cuoci, A. Parente, T. Faravelli, Examination of a soot model in premixed laminar flames at fuel-rich conditions, *Proc. Combust. Inst.* 37 (2019) 1013–1021.
- J.A. Miller, S.J. Klippenstein, From the multiple-well master equation to phenomenological rate coefficients: reactions on a C<sub>3</sub>H<sub>4</sub> potential energy surface, *J. Phys. Chem. A* 107 (2003) 2680–2692.
- J.A. Miller, J.P. Senosiain, S.J. Klippenstein, Y. Georgievskii, Reactions over multiple, interconnected potential wells: unimolecular and bimolecular reactions on a C<sub>3</sub>H<sub>5</sub> potential, *J. Phys. Chem. A* 112 (2008) 9429–9438.
- J.A. Miller, S.J. Klippenstein, Dissociation of propyl radicals and other reactions on a C<sub>3</sub>H<sub>7</sub> potential, *J. Phys. Chem. A* 117 (2013) 2718–2727.
- L. Ye, Y. Georgievskii, S.J. Klippenstein, Pressure-dependent branching in the reaction of 1CH<sub>2</sub> with C<sub>2</sub>H<sub>4</sub> and other reactions on the C<sub>3</sub>H<sub>6</sub> potential energy surface, *Proc. Combust. Inst.* 35 (2015) 223–230.
- D. Polino, S.J. Klippenstein, L.B. Harding, Y. Georgievskii, Predictive theory for the addition and insertion kinetics of 1CH<sub>2</sub> reacting with unsaturated hydrocarbons, *J. Phys. Chem. A* 117 (2013) 12677–12692.
- A.W. Jasper, N. Hansen, Hydrogen-assisted isomerizations of fulvene to benzene and of larger cyclic aromatic hydrocarbons, *Proc. Combust. Inst.* 34 (2013) 279–287.
- P.T. Lynch, C.J. Annesley, C.J. Aul, X. Yang, R.S. Tranter, Recombination of allyl radicals in the high temperature fall-off regime, *J. Phys. Chem. A* 117 (2013) 4750–4761.
- A. Fridlyand, P.T. Lynch, R.S. Tranter, K. Brezinsky, Single pulse shock tube study of allyl radical recombination, *J. Phys. Chem. A* 117 (2013) 4762–4776.
- K. Wang, S.M. Villano, A.M. Dean, Reactions of allylic radicals that im-



- pact molecular weight growth kinetics, *Phys. Chem. Chem. Phys.* 17 (2015) 6255–6273.
- [44] C. Huang, B. Yang, F. Zhang, Initiation mechanism of 1, 3-butadiene combustion and its effect on soot precursors, *Combust. Flame* 184 (2017) 167–175.
- [45] J.P. Lockhart, C.F. Goldsmith, J.B. Randazzo, B. Ruscic, R.S. Tranter, An experimental and theoretical study of the thermal decomposition of C<sub>4</sub>H<sub>6</sub> isomers, *J. Phys. Chem. A* 121 (2017) 3827–3850.
- [46] T.V. Pham, H.T.T. Trang, C.T. Ngo, H.M.T. Nguyen, A quantum chemical study of the mechanisms and kinetics of the reaction between propargyl (C<sub>3</sub>H<sub>3</sub>) and methyl (CH<sub>3</sub>) radicals, *Chem. Phys. Lett.* 762 (2021) 138126.
- [47] J. Zador, M.D. Fellows, J.A. Miller, Initiation reactions in acetylene pyrolysis, *J. Phys. Chem. A* 121 (2017) 4203–4217.
- [48] S. Sharma, W.H. Green, Computed rate coefficients and product yields for c-C<sub>5</sub>H<sub>5</sub>+ CH<sub>3</sub>→ products, *J. Phys. Chem. A* 113 (2009) 8871–8882.
- [49] V.S. Krasnouchkov, D.P. Porfiriev, I.P. Zavershinskiy, V.N. Azyazov, A.M. Mebel, Kinetics of the CH<sub>3</sub> + C<sub>5</sub>H<sub>5</sub> reaction: a theoretical study, *J. Phys. Chem. A* 121 (2017) 9191–9200.
- [50] G. da Silva, J.A. Cole, J.W. Bozzelli, Kinetics of the Cyclopentadienyl + Acetylene, Fulvenallene + H, and 1-Ethynylcyclopentadiene + H reactions, *J. Phys. Chem. A* 114 (2010) 2275–2283.
- [51] D. Trogolo, A. Maranzana, G. Ghigo, G. Tonachini, First ring formation by radical addition of propargyl to but-1-ene-3-yne in combustion. Theoretical study of the C<sub>7</sub>H<sub>7</sub> radical system, *J. Phys. Chem. A* 118 (2014) 427–440.
- [52] V. Kislov, A. Mebel, Ab initio G<sub>3</sub>-type/statistical theory study of the formation of indene in combustion flames. I. Pathways involving benzene and phenyl radical, *J. Phys. Chem. A* 111 (2007) 3922–3931.
- [53] F. Zhang, R.I. Kaiser, V.V. Kislov, A.M. Mebel, A. Golan, M. Ahmed, A VUV photoionization study of the formation of the indene molecule and its isomers, *J. Phys. Chem. Lett.* 2 (2011) 1731–1735.
- [54] L. Vereecken, H.F. Bettinger, J. Peeters, Reactions of chemically activated C<sub>9</sub>H<sub>9</sub> species. Part I. The product distribution of the reaction of phenyl radicals with propyne, *Phys. Chem. Chem. Phys.* 4 (2002) 2019–2027.
- [55] L. Vereecken, J. Peeters, Reactions of chemically activated C<sub>9</sub>H<sub>9</sub> species II: the reaction of phenyl radicals with allene and cyclopropene, and of benzyl radicals with acetylene, *Phys. Chem. Chem. Phys.* 5 (2003) 2807–2817.
- [56] B. Ruscic, Active thermochemical tables: sequential bond dissociation enthalpies of methane, ethane, and methanol and the related thermochemistry, *J. Phys. Chem. A* 119 (2015) 7810–7837.
- [57] A. Burcat, B. Ruscic, Third Millennium Ideal Gas and Condensed Phase Thermochemical Database for Combustion (with update from Active Thermochemical Tables), Argonne National Lab.(ANL), Argonne, IL (United States), 2005.
- [58] E.R. Ritter, J.W. Bozzelli, THERM: thermodynamic property estimation for gas phase radicals and molecules, *Int. J. Chem. Kinet.* 23 (1991) 767–778.
- [59] COSILAB The Combustion Simulation Laboratory, Rotexo GmbH & Co. KG, Haan, Germany, Version 3.3.2.
- [60] A. Comandini, T. Malewicki, K. Brezinsky, Chemistry of polycyclic aromatic hydrocarbons formation from phenyl radical pyrolysis and reaction of phenyl and acetylene, *J. Phys. Chem. A* 116 (2012) 2409–2434.
- [61] X. Han, M. Liszka, R. Xu, K. Brezinsky, H. Wang, A high pressure shock tube study of pyrolysis of real jet fuel Jet A, *Proc. Combust. Inst.* 37 (2019) 189–196.
- [62] W. Tang, K. Brezinsky, Chemical kinetic simulations behind reflected shock waves, *Int. J. Chem. Kinet.* 38 (2006) 75–97.
- [63] X. Han, J.M. Mehta, K. Brezinsky, Temperature approximations in chemical kinetics studies using single pulse shock tubes, *Combust. Flame* 209 (2019) 1–12.
- [64] C. Shao, G. Kukkadapu, S.W. Wagnon, W.J. Pitz, S.M. Sarathy, PAH formation from jet stirred reactor pyrolysis of gasoline surrogates, *Combust. Flame* 219 (2020) 312–326.
- [65] A. Fahr, A. Nayak, Kinetics and products of propargyl (C<sub>3</sub>H<sub>3</sub>) radical self-reactions and propargyl-methyl cross-combination reactions, *Int. J. Chem. Kinet.* 32 (2000) 118–124.
- [66] V.D. Knyazev, I.R. Slagle, Kinetics of the reactions of allyl and propargyl radicals with CH<sub>3</sub>, *J. Phys. Chem. A* 105 (2001) 3196–3204.
- [67] C.-W. Zhou, Y. Li, U. Burke, C. Banyon, K.P. Somers, S. Ding, S. Khan, J.W. Hargis, T. Sikes, O. Mathieu, E.L. Petersen, M. AlAbbad, A. Farooq, Y. Pan, Y. Zhang, Z. Huang, J. Lopez, Z. Loparo, S.S. Vasu, H.J. Curran, An experimental and chemical kinetic modeling study of 1,3-butadiene combustion: ignition delay time and laminar flame speed measurements, *Combust. Flame* 197 (2018) 423–438.
- [68] N. Hansen, X. He, R. Griggs, K. Moshhammer, Knowledge generation through data research: new validation targets for the refinement of kinetic mechanisms, *Proc. Combust. Inst.* 37 (2019) 743–750.
- [69] A.E. Long, S.S. Merchant, A.G. Vandeputte, H.-H. Carstensen, A.J. Vervust, G.B. Marin, K.M. Van Geem, W.H. Green, Pressure dependent kinetic analysis of pathways to naphthalene from cyclopentadienyl recombination, *Combust. Flame* 187 (2018) 247–256.
- [70] L. Zhao, R.I. Kaiser, B. Xu, U. Ablikim, M. Ahmed, M.V. Zagidullin, V.N. Azyazov, A.H. Howlader, S.F. Wnuk, A.M. Mebel, VUV photoionization study of the formation of the simplest polycyclic aromatic hydrocarbon: naphthalene (C<sub>10</sub>H<sub>8</sub>), *J. Phys. Chem. Lett.* 9 (2018) 2620–2626.
- [71] A. Matsugi, A. Miyoshi, Modeling of two- and three-ring aromatics formation in the pyrolysis of toluene, *Proc. Combust. Inst.* 34 (2013) 269–277.
- [72] H. Jin, L. Xing, J. Hao, J. Yang, Y. Zhang, C. Cao, Y. Pan, A. Farooq, A chemical kinetic modeling study of indene pyrolysis, *Combust. Flame* 206 (2019) 1–20.
- [73] B. Shukla, K. Tsuchiya, M. Koshi, Novel products from C<sub>6</sub>H<sub>5</sub>+ C<sub>6</sub>H<sub>6</sub>/C<sub>6</sub>H<sub>5</sub> reactions, *J. Phys. Chem. A* 115 (2011) 5284–5293.
- [74] B. Shukla, A. Miyoshi, M. Koshi, Role of Methyl Radicals in the Growth of PAHs, *J. Am. Soc. Mass. Spectr.* 21 (2010) 534–544.
- [75] M. Schenk, N. Hansen, H. Vieker, A. Beyer, A. Götzhäuser, K. Kohse-Höinghaus, PAH formation and soot morphology in flames of C<sub>4</sub> fuels, *Proc. Combust. Inst.* 35 (2015) 1761–1769.
- [76] B. Shukla, M. Koshi, Comparative study on the growth mechanisms of PAHs, *Combust. Flame* 158 (2011) 369–375.
- [77] N. Hansen, M. Schenk, K. Moshhammer, K. Kohse-Höinghaus, Investigating repetitive reaction pathways for the formation of polycyclic aromatic hydrocarbons in combustion processes, *Combust. Flame* 180 (2017) 250–261.